Colloids and Surfaces A 577 (2019) 645–673

Contents lists available at ScienceDirect

Colloids and Surfaces A

journal homepage: www.elsevier.com/locate/colsurfa

Improving the performance of oil based mud and water based mud in a high temperature hole using nanosilica nanoparticles

Allan Katende[a,c,e,*], Natalie V. Boyou[b], Issham Ismail[b], Derek Z. Chung[b], Farad Sagala[d], Norhafizuddin Hussein[b], Muhamad S. Ismail[b]

[a] Department of Energy, Minerals and Petroleum Engineering. Mbarara University of Science and Technology (MUST), Uganda
[b] Department of Petroleum Engineering, Faculty of Chemical and Energy Engineering, Universiti Teknologi Malaysia, Malaysia
[c] Department of Mechanical and Industrial Engineering, Mbarara University of Science and Technology (MUST), Uganda
[d] Department of Chemical and Petroleum Engineering, University of Calgary (UC), Canada
[e] Department of Geoscience and Petroleum, Norwegian University of Science and Technology (NTNU), Norway

GRAPHICAL ABSTRACT

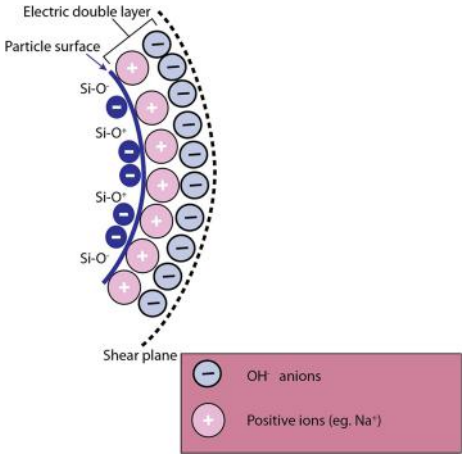

ARTICLE INFO

Keywords:
Nanosilica
Oil-based mud
Water-based mud
High pressure high temperature
Degradation
Rheological properties

ABSTRACT

Oil-based mud (OBM), a non-Newtonian fluid, is known for its superior performance in drilling complex wells as well as combating potential drilling complications. However, the good performance may degrade under certain circumstances especially because of the impact of chemical instability at an elevated temperature. The same phenomenon occurs for water-based mud (WBM) when it is used in drilling under high temperature conditions. To prevent this degradation from occurring, numerous studies on utilizing nanoparticles to formulate smart fluids for drilling operations are being conducted worldwide. Hence, this study aims to evaluate the performance of nanosilica (NS) as a fluid loss reducer and a rheological property improver in both OBM and WBM systems at high temperature conditions. This study focuses on the impacts of different nanosilica concentrations, varying from 0.5 ppb to 1.5 ppb, and different mud weights of 9 ppg and 12 pg as well as different aging temperatures, ranging from ambient temperature to 300 °F, on the rheological performance of OBM and WBM. All the rheological properties are measured at ambient temperature, and additionally tests, including lubricity, electrical stability, and high-pressure high-temperature filtration measurements, are conducted, and rheological models

* Corresponding author at: Department of Geoscience and Petroleum, Norwegian University of Science and Technology (NTNU), Norway.
E-mail addresses: allan_katende@hotmail.com, akatende@must.ac.ug, allank@alumni.ntnu.no (A. Katende).

https://doi.org/10.1016/j.colsurfa.2019.05.088
Received 28 March 2019; Received in revised form 29 May 2019; Accepted 30 May 2019
Available online 01 June 2019
0927-7757/ © 2019 The Authors. Published by Elsevier B.V. This is an open access article under the CC BY-NC-ND license (http://creativecommons.org/licenses/by-nc-nd/4.0/).

are obtained. The performance of nanosilica is then studied by comparing each of the nanosilica-enhanced mud systems with the corresponding basic mud system, taking the fluid loss and rheological properties as the benchmark parameters. Nanosilica shows a positive impact on OBM and WBM, as the presence of nanosilica in the mud systems can effectively improve almost all their rheological properties.

1. Introduction

Drilling fluid, more commonly known as drilling mud, is often used during drilling of subterranean wells. It aids drilling operations by cooling the drill bits and lubricating the process. This role makes the mixture fluid as vital to the development of petroleum resources as blood is to the human body [1–3] because almost 25% of expenditures for oilfield exploration are spent on drilling [4–8], and drilling without drilling fluid is barely practical. Drilling fluid has an extensive history in the oil and gas industry, which can be dated back to the third millennium [9,10]. Based on the history of drilling, water was the first drilling fluid utilized by the French almost two centuries ago [11], and today, water is still an important component [3,6] primarily used in drilling fluid formulation.

Generally, several types of drilling fluids are currently widely used, namely, oil-based drilling fluid, synthetic-based drilling fluid and water-based drilling fluid [3,12]. Because water-based drilling fluids are less expensive and more environmentally friendly [3,13,14], they are always preferred in drilling operations. However, under more complicated drilling conditions with the presence of shale in the formation, the drilling mud must maintain a high pressure and be able to tolerant a high temperature; thus, oil-based drilling fluids are often desired due to their superior drilling performance [15].

With the challenges and in the era of low oil prices, precise selection of the drilling fluid type and properties is essential to optimizing the drilling time and expenditure. Improved formulation and engineering design of drilling mud is constantly under development to improve water-based mud (WBM) for application in environmentally sensitive areas [3,12,15,16] and to prevent OBM from degradation, which will compromise its superior performance, due to the temperature effect.

In recent years, nanotechnology has aroused attention in the oil industry due to its vast applicability [17–23] and is being used in formulating drilling fluid, which is more often known as a nano-mud, to combat standing challenges and enhance the drilling performance [1,24–28]. A nano-mud can be simply defined as any drilling fluid whose composition includes at least one type of mud additive in the nanoparticle size range of 1–100 nm [15,29]. Due to the extremely tiny particle size, which results in an exceptionally high surface area to volume ratio [30], nanoparticles are often stronger and more reactive than non-nanoparticles [31–34].

These special characteristics of nanoparticles make them very unique, sensitive and chemically as well as physically reactive agents. Due to the tiny size of nanoparticles, they can act as great bridging agents, as they can effectively plug nanosized pores and prevent fluid loss especially to the shale formation, through which wellbore instability can be eventually prevented [35,36]. In addition, nanoparticles that have high sensitivity and reactivity with bentonite particles can improve and stabilize the rheological properties of drilling fluids, which will lead to better hole cleaning and cuttings suspension [15,25,37,38].

Because of the superior performance of nanoparticles, they are broadly applied in drilling fluid formulations, such as in WBM in order to enhance the environmentally and cost friendly drilling fluid to combat problems such as shale inhibition, fluid loss [39], lubricity and thermal stability [40], and in oil-based mud (OBM) to enhance its thermal stability and preserve or even enhance its properties at an elevated temperature. Scholars have been trying [99] to formulate enhanced WBM and OBM by using numerous special additives, including nanoparticles, to formulate a commercially inexpensive and environmentally suitable WBM and a more thermally stable and rheologically better OBM [15,41–43]. Therefore, considering the potential superior properties that nanoparticles can offer, nanosilica, a type of hydrophilic nanoparticle, is used in both WBM and OBM to study the effect of nanosilica on the rheological properties of both muds.

Drilling problems are the potential complications that arise during a drilling operation of a complicated well, which may be a deviated well or one in which a formation with the presence of shale layers or rock layers with different hardnesses has to be drilled through, which may result in a stuck pipe, shale swelling and well bore instability. Unsurprisingly, the root of all drilling problems is inseparable from the incapability of the current conventional drilling fluids used to fulfill particular functional tasks that are very vital in today's challenging environments involving both drilling and production [31,32,44–47].

Although OBM is often preferred for its superior performance in drilling a complicated well, as it can easily combat these drilling problems [48]; the macroscopic and microscopic types of additives are still very likely insufficient, as their properties can be altered under extreme temperature or pressure conditions either physically or chemically [31,32]. This issue has led the industry to switch to more attractive alternatives [12,49]: the application of WBM and OBM enhanced by nanotechnology. Thus, in this study, nanosilica is used as an enhancing nanosized additive to design water-based and oil-based nano-muds in order to achieve their functionalities from the commencement of the drilling process to its cessation.

2. Methodology

The methodologies in this study are based solely on laboratory experimental work. The rheological property tests are conducted according to the recommended practice of API RP 13B-1 [50] for examining a drilling fluid. The experimental plan is as shown in Fig. 1

2.1. Dispersion of nanoparticles

Any nanoparticles to be used as an additive of a drilling fluid need to be thoroughly dispersed prior to adding them to the drilling fluid [51,52] so that they work optimally. Riley et al. [28] assert that the dispersion of nanoparticles has to be stabilized to prevent the particles from agglomerating and precipitating.

Nanosilica (NS) is dispersed under a high pH condition so that anionic charge is acquired on the native silica. Charging the nanosilica's surfaces, as shown in Fig. 2, enables it to be self-repulsive, which leads to a good dispersion of nanosilica particles [53–55]. The working condition is then maintained at a pH above 9 to ensure that the nanosilica dispersion is stabilized.

2.2. Mud formulation

2.2.1. WBM formulation

The WBM in this study was prepared according to the Recommended Practice for Field Testing Water-Based Drilling Fluid (API RP 13B-1, 2009 [50]). The practice clearly states that 350 cc of WBM is equivalent to a laboratory barrel, and 15 lb/bbl of bentonite is used per laboratory barrel.

The standard WBM formulations for mud weights of 9 ppg and 12 ppg are tabulated in Tables 1 and 2.

Nomenclature

ρ	density
n	exponent
k	flow consistency index
μ_p	plastic viscosity
μ_d	dynamic viscosity
τ_y	yield stress
τ_o	initial shear stress
ES	electrical stability
ESV	electrical stability values
WBM	water based mud
OBM	oil based mud
NS	nano silica
API	American Petroleum Institute
LPLT	low pressure low temperature
HPHT	high pressure high temperature
PAC	polyanionic cellulose
PV	plastic viscosity
YP	yield point
ROP	rate of penetration
T	temperature
GS	gel strength
AHR	after hot rolling
BHR	before hot rolling
CoF	coefficient of friction

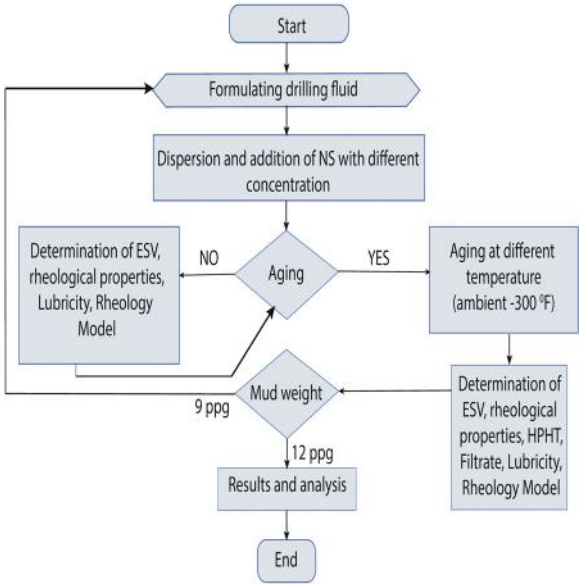

Fig. 1. Experimental methodology.

2.2.2. WBM formulation with nanosilica

In this study, rheological property, low-pressure low-temperature (LPLT) filtration, high-pressure high-temperature (HPHT) filtration and lubricity tests are performed, and rheological models are obtained. The performance of WBM with nanosilica is compared with that of its basic mud. The procedure for formulating the nano-WBM is as follows:

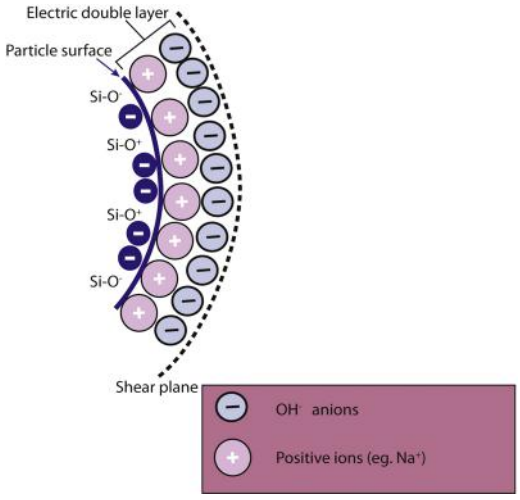

Fig. 2. Charging of the nanosilica surface to enable self-repulsion.

Table 1
Standard water-based mud formulation for 9 ppg mud weight.

Additives	Function	Composition
Fresh water	Base fluid	332 cc
Soda ash	Treat water for contamination	0.25 cc
Bentonite	Viscosifier	15 cc
PAC-HV	Fluid loss control agent	0.2 cc
Hydroxypropyl Starch(HS)	Fluid loss control agent	1.5 g
Caustic soda	pH controller	0.25 g
Barite	Weighting agent	27.99 g

Table 2
Standard water-based mud formulation for 12 ppg mud weight.

Additives	Function	Composition
Fresh water	Base fluid	293 cc
Soda ash	Treat water for contamination	0.25 cc
Bentonite	Viscosifier	15 cc
PAC-HV	Fluid loss control agent	0.2 cc
HS	Fluid loss control agent	1.5 g
Caustic soda	pH controller	0.25 g
Barite	Weighting agent	193.43 g

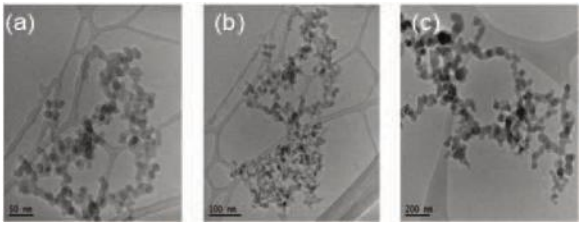

Fig. 3. TEM images of nanosilica in alkaline solution with different concentrations: (a) 0.5 ppb, (b) 1.0 ppb, (c) 1.5 ppb.

1. Nanosilica of respective concentrations (0.5, 1.0, and 1.5 ppb) are dispersed into 100 cc of distilled water with 0.25 g of caustic soda mixture (alkaline solution). Transmission Electron Microscope (TEM) images of these mixtures are portrayed in Fig. 3. Results showed that they are well dispersed, and this is proven with zeta potential values in Table 7, as the absolute values for all three nanosilica concentration in the alkaline solution are well over 30 mV.
2. Calculated amount of water – 100 cc of water is weighed using an electronic balance and then poured into a mixer cup; in this study, 193 cc (293–100 cc) of water is used.

3. The water is stirred using a multi-mixer while 0.25 g of soda ash is added into the water. Two minutes are counted from the beginning of the stirring.
4. At the end of the two minutes, 15 g of bentonite is added, and the solution is then stirred for five minutes.
5. A total of 0.2 g of high viscosity polyanionic cellulose (PAC-HV) is added, and the solution is stirred for three minutes.
6. Next, 1.5 g of hydroxypropyl starch is added, and the mixture is stirred for three minutes.
7. The nanosilica solution is added into the mixture and then stirred for 10 min.
8. The stirring is continued until, at the 35th minute, the calculated amount of barite is added in order to formulate a mud sample of 9 or 12 ppg; the mixture is then stirred throughout the remaining time. The entire mixing process of the mud takes 45 min.

2.2.3. OBM formulation

Standardized OBM with an oil-to-water ratio of 80:20 is formulated for all tests throughout the study. The compositions of the OBM are illustrated in Table 3 and 4.

2.3. Rheological property test

The rheological properties of a mud sample, such as the plastic viscosity (PV), yield point (YP), 10 s gel strength (10 s GS), 10 min gel strength (10 m GS), are all measured with the aid of a FANN Viscometer. All these tests are repeated before and after aging at a temperature range from 77 to 300 °F for two different mud weights (9 ppg and 12 ppg).

Table 5 shows the recommended rheological properties, which were utilized to evaluate the performance of all the formulated samples.

2.4. Rheological model

Rheological models of mud samples were obtained using a Brookfield RST Touch^{TM} Rheometer both before and after aging to investigate the effect of temperature on the rheological model of the mud samples and study the effect of nanosilica on both WBM and OBM.

Table 3
Standard oil-based mud formulation for 9 ppg mud weight.

Additives	Function	Composition
Sarapar 147	Base oil	182.09 cc
Confimul P	Primary emulsifier	5 cc
Confimul S	Secondary emulsifier	5 cc
Distilled water	Liquid phase	59 cc
Calcium chloride	Reactive clay stabilliser	8.65 g
Confi-gel	Viscosifier and gelling agent	5 g
Confi-trol	Fluid loss control agent	7 g
Lime	pH controller	4 g
Barite	Weighting agent	103.53 g

Table 4
Standard oil-based mud formulation for 12 ppg mud weight.

Additives	Function	Composition
Sarapar 147	Base oil	159.77 cc
Confimul P	Primary emulsifier	5 cc
Confimul S	Secondary emulsifier	5 cc
Distilled water	Liquid phase	52 cc
Calcium chloride	Reactive clay stabilliser	7.58 g
Confi-gel	Viscosifier and gelling agent	5 g
Confi-trol	Fluid loss control agent	7 g
Lime	pH controller	4 g
Barite	Weighting agent	260.22 g

Table 5
Recommended rheological properties suggested by Li et al. [56,57].

Rheological property	Specification
Electrical stability, V	400, as high as practicable
Plastic viscosity, cp	10–60, preferably 15–40
Yield point, lb/100 sq. ft	2.5–20, preferably 5–12.5
Gel strength (10 s)	4–10
Gel strength (10 min)	4–15
HPHT fluid loss, cc	< 10

2.5. Lubricity test

The lubricity test was conducted on mud samples both before and after aging using an OFITE Lubricity Tester to investigate the effect of temperature on the lubricity of the mud samples. The lubricity of a mud sample can be determined by measuring the coefficient of friction (CoF) of the sample with a lubricity test. This test utilizes the concept of metal-to-metal contact to simulate the drill string and wellbore condition. Lubricity is calculated by the following equations.

$$\text{Coeficient factor} = \frac{\text{Meter reading using deionised water}}{34} \quad (1)$$

$$\text{Lubricity Coefficient CoF} = \frac{\text{CF(Meter reading from } a \text{ mud sample)}}{100} \quad (2)$$

$$\text{Relative CoF reduction} = \frac{\text{CoF}_{\text{basic mud}} - \text{CoF}_{\text{nanosilica}}}{\text{CoF}_{\text{basic mud}}} \quad (3)$$

2.6. Electrical stability (ES) test

The ES test is carried out to examine the OBM emulsion and oil-wetting qualities of mud samples. ES is measured by generating a gradually increasing sinusoidal alternating voltage across a pair of electrodes submerged in the OBM samples.

2.7. Transmission electron microscop (TEM) and Zeta potential characterization of nanosilica

The nanosilica used in this study was procured and prepared by Shanghai Honest Chem Co., Ltd, China. No further modifications were made prior to testing. The properties of nanosilica are listed in Table 6. The particle size of nanosilica is approximately 14 nm and round in shape as observed in TEM images (Fig. 3).

Table 7 shows the Zeta potential measurement and Fig. 3 shows the transmission electron microscopy (TEM) images of the 14 nm nanosilica

Table 6
Properties of nanosilica.

Properties	Specifications
Appearance	White powder
Density	2.4 g/cm^3
Purity of SiO2	99.90%
Particle size	14 nm
pH (5% suspension)	4.5
Heating loss (105 °C for 2 h)	0.90%
Ignition loss (1000 °C for 2 h)	1.20%
Absorption value	230 ml/100 g
Specific surface area	202 m^2/g
Heavy metals	< 0.001 %
Sodium sulphate	< 0.02 %
Lead content	< 0.0001 %
Iron (Fe)	149 mg/kg
Manganese (Mn)	3 mg/kg
Copper	1 mg/kg
Arsenic	< 0.00001%

Table 7
Average zeta potential values with different nanosilica concentrations.

Sample type	T [°C]	Zeta potential (ζ) [mV]
Water + caustic soda + Nano 0.5 ppb	25.1	−42.2
Water + caustic soda + Nano 1.0 ppb	25	−43.4
Water + caustic soda + Nano 1.5 ppb	25	−43.9

tested in an alkaline solution of 100 ml distilled water with 0.25 ppb of caustic soda. The nanosilica used in this study was spherical in shape and these images showed well dispersions of nanosilica without the need for long ultrasonication.

According to Wissing et al. [58] and Kavitha et al. [59], absolute zeta potential values above 30 mV provide good dispersion and stability. Meanwhile, zeta potential values of above 60 mV and around 20 mV provide excellent stability and short-term stability respectively (Honary and Zahir [60]). This study shows that different concentrations of nanosilica produced almost similar zeta potential values. There was a slight increase in zeta potential values when nanosilica increases. All samples in Table 7 generated high zeta potential values (> 30 mV) which suggests good and stable dispersions.

2.8. Field emission scanning electron microscope (FESEM) analysis

The mud cake is thicker for muds with nanosilica because as nanosilica plugged the pore spaces of the filter paper, water was still able to seep through the hydrophilic layer of nanosilica [61]. Thus, resulted in thicker mud cake. This also explained why filtrate volumes of muds with nanosilica was slightly higher than muds without nanosilica.

FESEM results in Fig. 4 show that 9 ppg WBM and OBM produces slightly smother surfaces compared to 9 ppg WBM and OBM with nanosilica. Based on the images, nanosilica was still in their nanosized state after they were mixed in the fluids.

3. Results and discussions

3.1. Rheological properties of OBM samples

3.1.1. ES test

Fig. 5 shows the ES of the 9 ppg OBM samples with and without nanosilica, with the concentration ranging from 0–1.5 ppb. The samples

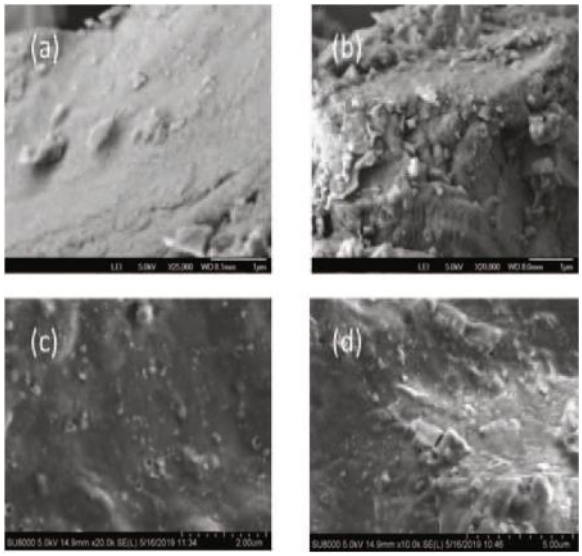

Fig. 4. FESEM images of (a) WBM 9 ppg, (b) WBM 9 ppg with 1.0 ppb nanosilica, (c) OBM 9 ppg, (d) OBM 9 ppg with 1.0 ppb nanosilica.

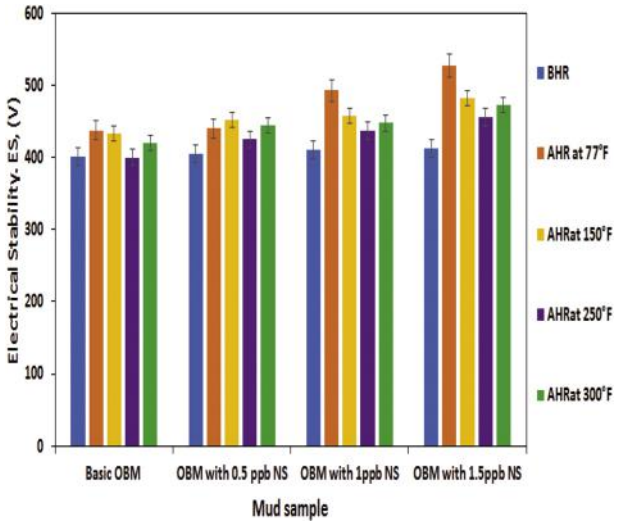

Fig. 5. ES of 9 ppg OBM samples with and without nanosilica.

were tested before the hot rolling process and after the hot rolling process under 100 psi at respective temperatures ranging from 77 °F to 300 °F (API RP 13B-1, 2009 [50]).

Sarapar 147 (see Table 18), the base oil used in formulating the OBM, consists of 96% (minimum) n-paraffins, < 5% iso-paraffins, < 0.1% napthanics, and < 0.01% aromatics. It has density of 775 kg/m^3 with boiling range from 258 °C to 293 °C. As observed from Fig. 5, all the OBM samples exhibit ES values equal to or greater than 400 V. According to the guidelines, these samples are practical, as the ES values imply that the emulsion system is stable. Additionally, other trends can be observed from the figure: all the ES values increase after aging and increase with increasing nanosilica concentration. This phenomenon occurs because the emulsifiers were protected (Growcock et al. [62]) even after hot rolling with the addition of nanosilica due to its high thermal stability. According to Growcock [62], the dispersed nanosilica will wrap and form an insulating film around the emulsifiers, protecting them from thermal degradation. This is true for OBM samples which were hot rolled from 77 °F till 250 °F.

In accordance with kinetic theory [63], when mud samples undergo hot rolling at a high temperature range of 250 °F to 300 °F (API RP 13B-1, 2009 [50]), additive particles, including nanosilica, will be more kinetically active, resulting in poor formation of an insulating film, which causes a slight decrease in the ES values obtained. But Fig. 5 shows that all OBM samples increase after they were hot rolled at 300 °F. The theory is valid as long as the OBM sample is still in liquid form. As Sarapar 147 s (see Table 18) boiling point is 293 °F, and above that point it appears as vapour. Coupled with continuous hot-rolling process, this allows the insulation process to happen in a more positive form for all the OBM samples and subsequently results in a better ES reading as shown in Fig. 5. This new finding opens a window for further experimental investigation.

3.1.2. PV of 9 ppg OBM samples with and without nanosilica

Fig. 6 portrays the PV of the 9 ppg OBM samples with nanosilica as an additive before aging. According to Salih [15], the PV of a mud should decrease with the addition of nanoparticles, as the nanosized particles will act as “ball bearings” and be arranged among the larger particles of other additives such that less friction occurs.

Fig. 6 shows that with the addition of 0.5 ppb, 1 ppb and 1.5 ppb nanosilica, the PV decreases from 28 cp to 20 cp, 22 cp and 24 cp, respectively. The greatest reduction of the PV is observed with the addition of 0.5 ppb nanosilica. At 1.0 and 1.5 ppb nanosilica, the mud samples experience a lower reduction because more solid content is present in the mud systems, and less reduction of fiction is obtained

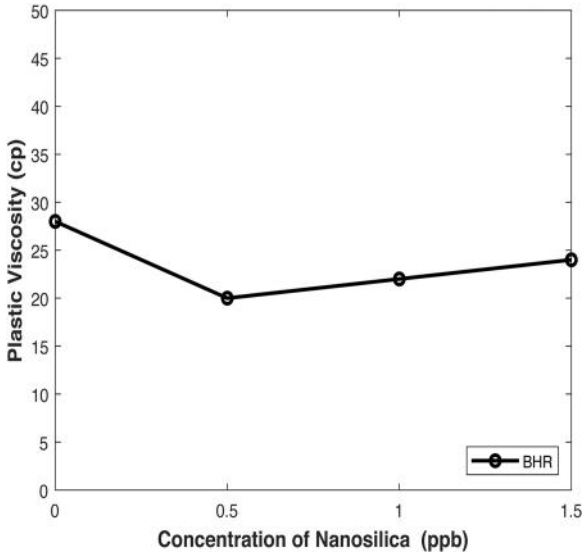

Fig. 6. PV of 9 ppg OBM samples before aging.

because of the constant collision of the mud particles within the system (Salih [15]).

Although all the reduced PV values obtained are all in the recommended range when nanosilica is used as an enhancing additive, the mud sample with the lowest PV value within the recommended range should be adopted because the minimum PV is often preferred in drilling operations in order to escalate the rate of penetration (ROP), reduce the energy needed for mud circulation, provide better cooling and lubrication functions to the downhole equipment and eventually diminish the mud loss during the circulation process resulting from the unexpected excessive equivalent circulation density that may give rise to formation fractures [15,64].

A reduction in PV is observed as soon as 0.5 ppb of nanosilica was added into the mud. This reduction is due to the ability of nanosilica to disrupt gel formations between particles in the mud [61]. The presence of nanosilica could help reduce PV for low and high mud weights and enables rapid drilling. Results show that as concentration of nanosilica increases to 1.0 and 1.5 ppb, PV increases as well. This increase was due to an increase in solid particles in the mud.

In low mud weights, the attractive forces of the particles in the mud are not as high as in high mud weights. Thus, in low mud weights, nanosilica helps increase gel formations which increase YP readings. In high mud weights however, the presence of 0.5 and 1.0 ppb concentration of nanosilica disrupts gel formations of other particles in the mud. Thus, a higher concentration of nanosilica is required for higher mud weights. In this case, 12 ppg mud requires a minimum concentration of 1.5 ppb of nanosilica for optimum YP performance.

Fig. 7 shows the PVs of 9 ppg OBM samples after aging at their respective temperature under 100 psi for 16 h.

Fig. 7 shows that the PVs of the OBM samples are high after aging, and higher PV values are obtained when the samples are aged at a higher temperature. This increase in the PV occurs because when the samples are aged at a higher temperature, the particles in the mud will be more kinetically active, which will result in more shear within the mud system itself (Paramasivam [65]) and eventually lead to an increase of the PV with increasing aging temperature.

All the OBM samples exhibit the same trends before aging and after aging. For all the samples, both before and after aging at their respective temperature, the PVs decrease when nanosilica is added.

After aging at 77 °F, the OBM sample with the addition of 0.5 ppb nanosilica shows a reduction in PV value from 30 cp to 21 cp, while the addition of 1.0 ppb nanosilica results in a decrease from 30 cp to 23 cp, and with 1.5 ppb nanosilica usage, a decrease from 30 cp to 25 cp is

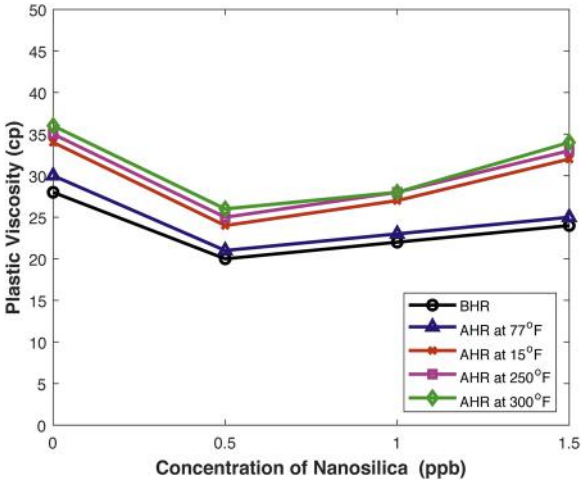

Fig. 7. PV of 9 ppg OBM samples after aging.

obtained.

As for the PVs obtained after aging at 150 °F, the usage of 0.5 ppb, 1.0 ppb and 1.5 ppb nanosilica results in a decrease of the PV from 34 cp to 24 cp, 27 cp and 32 cp, respectively. Similarly, the samples that undergo aging at 250 °F demonstrate a decline in the PV when nanosilica is added. When 0.5 ppb, 1.0 ppb and 1.5 ppb nanosilica is added into the OBM samples, a reduction from 35 cp to 25 cp, 28 cp and 33 cp is obtained, respectively.

When the OBM samples are aged at 300 °F, with the addition of 0.5 ppb, 1.0 ppb and 1.5 ppb nanosilica, a reduction of PV from 36 cp to 26 cp, 28 cp and 34 cp is obtained, respectively. All the samples show the greatest reduction in PV when 0.5 ppb nanosilica is used, which shows that 0.5 ppb is the optimum concentration for the PV. Agglomeration of nanosilica occurs above this concentration, leading to an increase in the PV.

3.1.3. YP of 9 ppg OBM samples with and without nanosilica

Fig. 8 shows the YP of the 9 ppg OBM samples when nanosilica is used as the enhancing additive with concentrations of 0.5 to 1.5 ppb before aging. According to the recommended specification from previous studies [56,57], the ideal YP for an OBM should be in the range of 5–12.5 lb/100 sq ft.

The YP is defined as the minimum force required to transform drilling fluid to the gel condition to the flowing condition as soon as it has become motionless [9] and is precisely referred to as the cuttings carrying capacity of the drilling fluid [6,7,9,61,66–68]. The YP of a

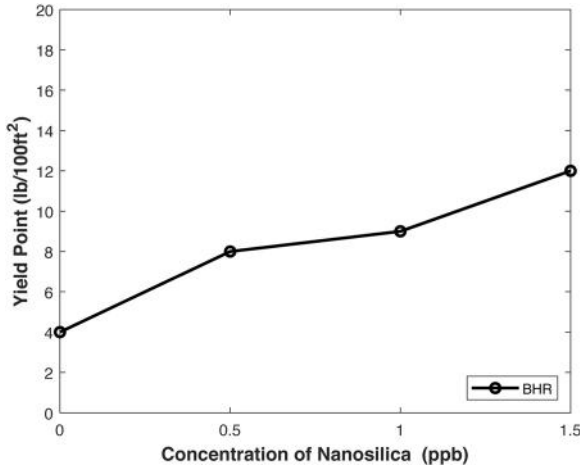

Fig. 8. YP of 9 ppg OBM samples before aging.

drilling mud must be within the recommended range, as when a mud exceeds this range and reaches a fairly high YP, flocculation occurs, and a high YP further results in the unnecessary loss of pump pressure, a decrease in the ROP and an increase in the surge and swap pressure [15,69,70]. Unfortunately, an excessively low YP is also undesirable, as it will lead to sagging of barite.

Referring to Fig. 8, all the nanosilica-enhanced samples are within the recommended range except for one sample, the basic mud, as it has a low YP below the recommended range. Sagging of barite may be encountered if the basic mud sample is put into practice. When 0.5 ppb nanosilica is added, the YP value rises from 4 lb/100 sq ft to 8 lb/100 sq ft. As the concentration of nanosilica increases up to 1.0 ppb and 1.5 ppb, the YP values increase from 4 to 9 lb/100 sq ft and 12 lb/100 sq ft, respectively.

The increase of the YP after the addition of nanosilica and the directly proportional trend can be explained by the theory that there is a higher attractive force in the mud system with nanosilica. This higher attractive force is contributed by the huge surface area of nanosilica, as this will lead to a superior chemical reactivity, which eventually increases the YP of the nanosilica-enhanced mud samples [26,71–74].

Fig. 9 presents the YPs obtained for the 9 ppg OBM samples after the mud samples with and without nanosilica have gone through the aging process for 16 h under 100 psi at their respective temperature. The YP values obtained before aging are also plotted for a clearer comparison.

From Fig. 9, a trend of increasing YP values is obtained with increasing nanosilica concentration. This result is similar to the trend observed for the OBM samples before aging. After the samples are aged at 77 °F, a few samples lie within the recommended range of the ideal YP: the basic mud sample and OBM samples with 0.5 and 1.0 ppb nanosilica; the mud sample with 1.5 ppb nanosilica unfortunately no longer falls in the range. The YP values obtained when 0.5 ppb, 1.0 ppb and 1.5 ppb nanosilica is used as an additive show an increase from 5 lb/100 sq ft to 9 lb/100 sq ft, 11 lb/100 sq ft and 15 lb/100 sq ft, respectively.

When the aging temperature is increased to 150 °F, 3 samples also fall into the ideal range of the YP: the basic mud sample and OBM samples with 0.5 and 1.0 ppb nanosilica. In contrast, the sample with 1.5 ppb nanosilica has a YP that exceeds the recommended specification. When 0.5 ppb, 1.0 ppb and 1.5 pbb nanosilica is used as an additive, the YP of the basic mud is increased from 5 lb/100 sq ft to 11 lb/100 sq ft, 12 lb/100 sq ft and 16 lb/100 sq ft.

When the OBM samples undergo aging at 250 °F, only two samples remain in the ideal range, namely, the basic mud sample and the sample with 0.5 ppb nanosilica. With the addition of 0.5 ppb nanosilica, the YP value of the basic mud increases from 6 lb/100 sq ft to 12 lb/100 sq ft. However, a further increase in the nanosilica concentration promotes a further increase of the YP of the mud samples such that it no longer falls within the ideal range. The mud sample with 1.0 ppb nanosilica has a YP of 14 lb/100 sq ft, while that with 1.5 ppb nanosilica has a YP of 17 lb/100 sq ft.

A similar scenario occurs when the OBM samples are tested after aging at 300 °F for 16 h. The YP range recommended by the previous researchers [56,57] is from 5–12.5 lb/100 sq ft; however, the precision of a viscometer only goes to 1 unit, so 12.5 is rounded off to 13 lb/100 sq ft. For this range, only two samples fall within the specification, the basic mud sample and the OBM sample with 0.5 ppb nanosilica, as their YPs are 7 lb/100 sq ft and 13 lb/100 sq ft, respectively. As for the samples with nanosilica concentrations of 1.0 and 1.5 ppb, their YP values of 15 lb/100 sq ft and 18 lb/100 sq ft exceed the recommended range.

Paramasivam [65] claimed that a larger minimum force will be required at higher temperature conditions. This phenomenon occurs when OBM samples are tested after aging, as the YP values obtained are higher than those before aging. Additionally, the samples exhibit a pattern in which the YP values are higher when their aging temperature is higher. Overall, the highest YP within the range is always desirable because it promotes the efficient cuttings lifting of a drilling fluid, while a lower value may result in sagging of barite, and sagging is a very complicated issue [57,56]. In our case, 0.5 ppb nanosilica is the optimum concentration for obtaining the highest YP value within the recommended range.

3.1.4. GS at 10 s of 9 ppg OBM samples with and without nanosilica

The GS is defined as the capability of a drilling fluid to develop and maintain a gel structure as soon as the drilling operation comes to a halt (Paramasivam [65]). The GS is a measurement of the shear stress after the gel has set quiescently for some time [75–77]. A good GS is always required, as it would maintain the excessive circulation pressure needed to restart drilling operations [29,78,79].

Fig. 10 shows that the 10 s GSs of all OBM samples are within the recommended specification. No specific trend can be observed regarding the impact of temperature on the 10 s GS of the mud samples.

3.1.5. GS at 10 m of 9 ppg OBM samples with and without nanosilica

Fig. 11 demonstrates the 10 m GSs of OBM sample with and without nanosilica both before and after aging at their respective aging temperature. The ideal range of the 10 m GS suggested by previous researchers [56,57] is from 4 to 15 lb/100 sq ft.

Referring to Fig. 11, the 10 m GSs of almost all samples are in the recommended range except for the OBM samples with 1.0 and 1.5 ppb nanosilica that have undergone aging at 150 °F and the sample with

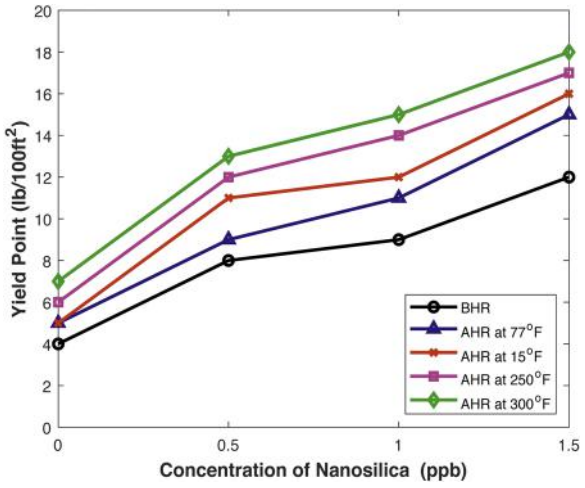

Fig. 9. YP of 9 ppg OBM samples after aging.

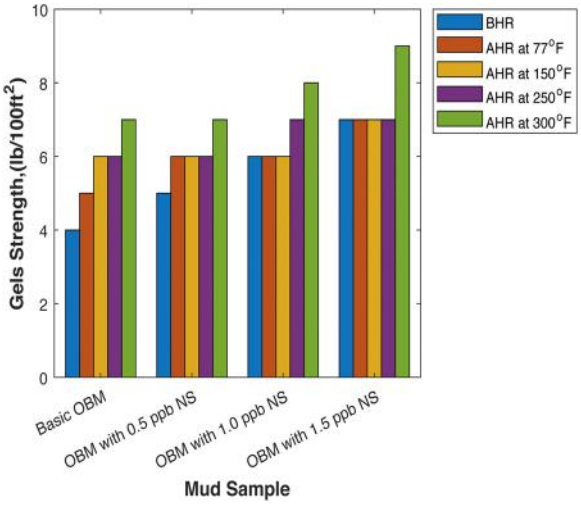

Fig. 10. GS at 10 s of 9 ppg OBM samples with and without nanosilica.

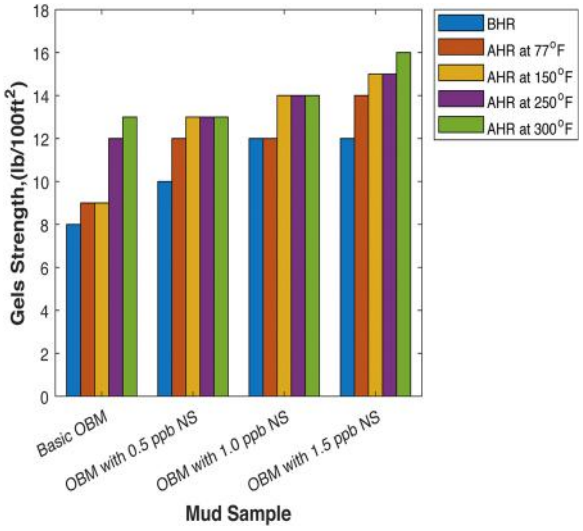

Fig. 11. GS at 10 m of 9 ppg OBM samples with and without nanosilica.

1.5 ppb nanosilica that has been aged at 300 °F; these samples have a 10 m GS of 16 lb/100 sq ft. Additionally, no specific pattern can be observed for the 10 m GS, and the impact of temperature is not significant enough to produce a trend in the 10 m GS.

The mud samples should have both the 10 s and 10 m GSs within the recommended ranges because excessive GSs can often result in swabbing and surging during run in hole and pull out of hole. Excessive GSs can also make the process of running in logging tools difficult and result in a tendency toward retaining and trapping sands, cuttings and air in the mud during drilling operations [75–77]. On the other hand, GS values lower than the ideal range will result in the formation of a too fragile gel [15], which is undesirable, as these mud samples will not have enough gel to suspend cuttings when the mud circulation or drilling operation is brought to a halt. The cuttings or even barite will suffer from sagging.

Fig. 12 shows a comparison of the 10 s and 10 m GSs of each set of OBM samples before and after aging at their respective temperature. The purpose of this comparison is to investigative if a particular OBM sample can form a progressive gel such that the ability to suspend cuttings when there is a pause in drilling would be promoted and the ability to break the gel and start flowing when drilling is resumed would be realized. Progressive gels are formed when there is a reasonably wide range between the initial (10 s) and 10 min gel readings [2,26].

Referring to Fig. 12(a)–(e), a trend can be observed, in which the 10 m GS is almost twice the 10 s GS. This result is desirable and proves the theory of Amani et al. [80]. In addition to ensuring the formation of progressive gels, this comparison is significant for ensuring that the development of high-flat gels or low-flat gels, for which both the 10 s GS and 10 m GS are high or low with no appreciable difference in the range between them, is avoided.

3.1.6. HPHT filtration of 9 ppg OBM samples with and without nanosilica

Fig. 13 displays the results of the HPHT filtration test conducted on the 9 ppg OBM samples with nanosilica concentration from 0.5 ppb to 1.5 ppb; however, the fluid loss after aging is only determined for those samples that have undergone high temperature aging (from 250 °F to 300 °F).

The recommended specification for an HPHT filtration test by researchers [56,57] is that the filtrate volume be less than or equal to 10 cc after 30 min of testing.

From Fig. 13, a pattern can be observed in which when nanosilica is added, the filtration increases with increasing nanosilica concentration. All the samples fulfill the ideal specification of having an HPHT filtration loss of less 10 cc.

Referring to the OBM samples aged at 250 °F, when 0.5 ppb nanosilica is added, the HPHT filtrate volume obtained at the end of 30 min is 2.2 cc, while the filtrate obtained from the basic mud is only 1.8 cc. A further increase in the nanosilica concentration leads to a further escalation of the HPHT fluid loss, reaching 3.0 cc and 3.4 cc when 1.0 ppb and 1.5 ppb nanosilica is added, respectively.

The same trend can be observed for the OBM samples aged at 300 °F. The usage of nanosilica causes a greater HPHT fluid loss, in which the basic mud only experiences a 3.0 cc fluid loss, while the mud samples with 0.5 ppb, 1.0 ppb and 1.5 ppb nanosilica undergo a filtration loss of 3.4 cc, 4.4 cc and 4.8 cc, respectively.

An increase in the temperature also increases the fluid loss of the mud samples; for instance, the OBM samples aged at 300 °F have greater fluid loss than those aged at 250 °F. This increase may occur because irregular flocculation of solid particles occurs at an elevated temperature [1,81,82], which worsens the fluid loss of the samples.

According to Wahid et al. [83], an increase in the nanosilica concentration will result in an adverse effect on the filtration properties. Nanosilica's inability to prevent fluid loss may be due to its overly small size [84], as the nanosilica used in this study is only 14 nm in size, while the pore size of the filter paper is 60 m; hence, the nanosilica will flow out together with the filtrate, resulting in almost no positive impact on combating fluid loss.

Salih [15] stated that flocculation promotes linking of the solid particles in mud systems in an edge-to-edge as well as edge-to-face manner, which will result in the formation of an open network structure that favors fluid loss. This theory matches the results in this study because the usage of nanosilica as well as a higher temperature generally increases the YP of a sample, which may lead to a very minor flocculation process.

3.1.7. Mud cake thickness of 9 ppg OBM samples with and without nanosilica

A filter cake or a mud cake will form at the wellbore across the permeable zone when filtrate loss occurs from the wellbore into the formation through the permeable zone. Excess filtration loss may result in formation damage. Thus, for any practical mud formulation, formation of a thin strong impermeable filter cake as filtration occurs is necessary to avoid further formation contamination resulting from filtrate loss and a blocked pipe due to an uneven or overly thick mud cake (Paramasivam [65]).

Fig. 14 portrays the thickness of the mud cakes formed during filtration for the OBM samples that have been aged at the high temperature of 250 °F or 300 °F. The figure shows that the thickness of the mud cake obtained is closely related or even directly proportional to the filtration volume. At a higher aging temperature, a higher filtrate loss volume is obtained, which contributes to thicker mud cake formation. With increasing nanosilica concentration, the YP of the mud samples increases, leading to very minor flocculation, which results in failure of impermeable mud cake formation and of fluid loss retainment.

3.1.8. Lubricity of 9 ppg OBM samples with and without nanosilica

The lubricity of a drilling mud is one of the important properties that should be governed during mud formulation, as the mud helps lubricate the drill string as drilling progresses [85,86]. The CoF is defined as the ratio of the frictional forces of two bodies that press against each other [9,78,87,88].

Fig. 15 shows the CoF values and Fig. 16 shows the reductions in the CoF relative to the basic mud of the 9 ppg OBM samples with and without nanosilica before and after aging at the respective aging temperature. An obvious trend can be observed when nanosilica is added into the mud samples. With the addition of nanosilica, the nano-muds exhibit lower CoF values compared to the basic mud, both before and after aging. The reduction in the CoF values relative to the basic mud is directly related to the nanosilica concentration; a lower CoF value is

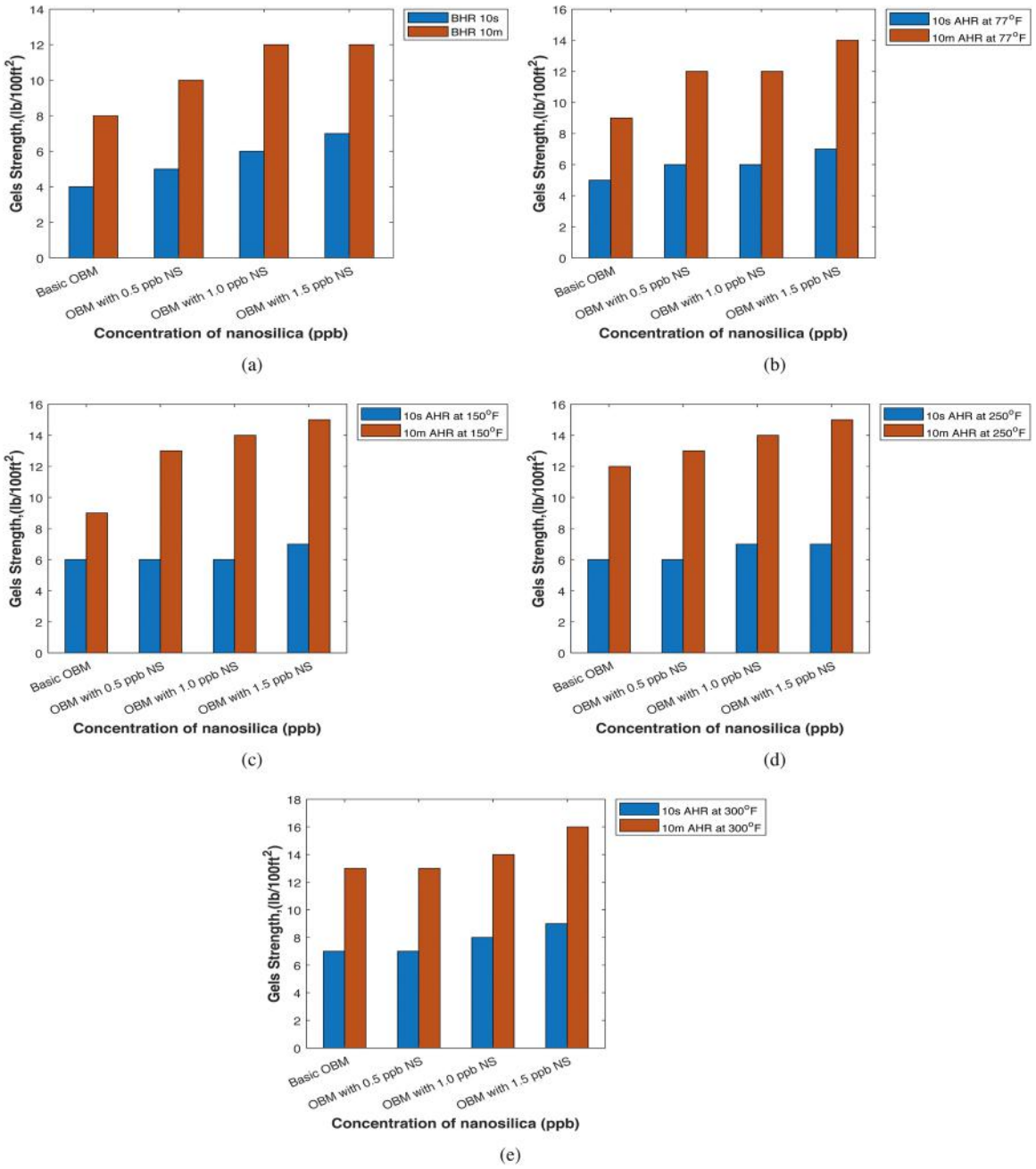

Fig. 12. Comparison of the 10 s and 10 m GSs of 9 ppg OBM samples with different aging temperatures: (a) before aging, (b) after aging at 77 °F, (c) after aging at 150 °F, (d) after aging at 250 °F and (e) after aging at 300 °F.

obtained when a higher concentration of nanosilica is added into the mud.

For example, before aging, with the addition of 0.5 ppb, 1.0 ppb and 1.5 ppb nanosilica to the OBM samples, relative CoF reductions of 1.4%, 2.8% and 3.3% are obtained, respectively. A similar trend is witnessed for the samples aged at ambient temperature, in which 4.6%, 6.6% and 7.9% reductions in the CoF relative to the basic mud are obtained when 0.5 ppb, 1.0 ppb and 1.5 ppb nanosilica is used. After aging at 150 °F, the OBM samples with nanosilica concentrations of 0.5 ppb, 1.0 ppb and 1.5 ppb show relative CoF reductions of 4.4%, 5.3% and 6.8%, respectively.

The highest reduction in the CoF is obtained for the samples that have undergone the 250 °F aging process. The highest reduction of 10.2% is obtained with the addition of 1.5 ppb nanosilica to the mud samples. As for the samples that have undergone aging at 300 °F, slight relative CoF reductions of 2.9%, 3.5% and 4.1% are obtained with the addition of 0.5 ppb, 1.0 ppb and 1.5 ppb nanosilica, respectively.

The lubricity of the drilling mud samples solely depends on the nanosilica concentration, while the temperature does not have an impact on it. Nanosilica has the ability to increase the lubricity of a mud by forming a boundary type of lubrication via physisorption [89,90]. The dispersed nanosilica will form a thin film and completely cover the metal surface of the lubricity tester. An increase in the concentration will favor the formation of the thin film, which will lubricate surfaces like ball bearings [15].

3.1.9. Electrical stability (ES) of 12 ppg OBM samples with and without nanosilica

Fig. 17 shows the results of the ES test conducted on the 12 ppg OBM samples with and without nanosilica both before and after aging

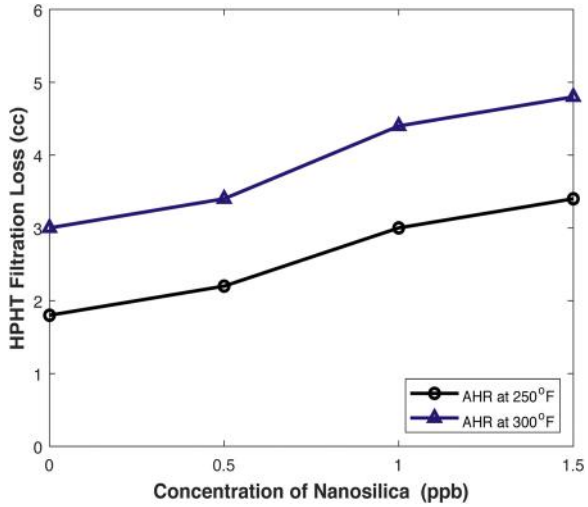

Fig. 13. HPHT filtration of 9 ppg OBM samples with and without nanosilica.

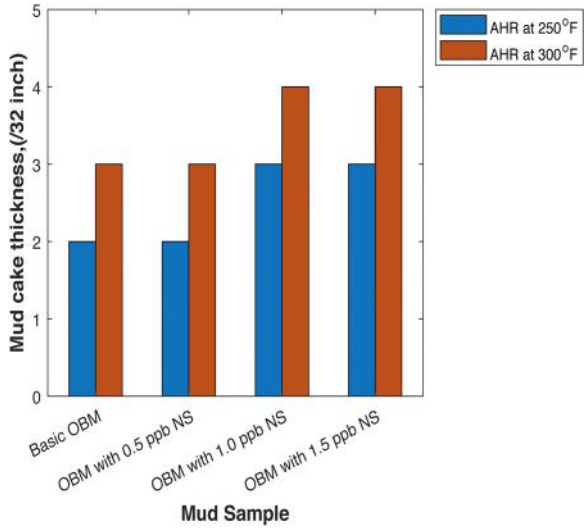

Fig. 14. Mud cake thickness of 9 ppg OBM samples with and without nanosilica.

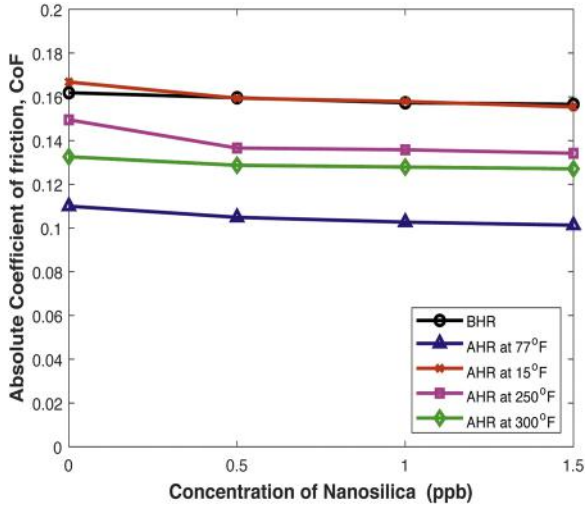

Fig. 15. CoF of 9 ppg OBM samples with and without nanosilica.

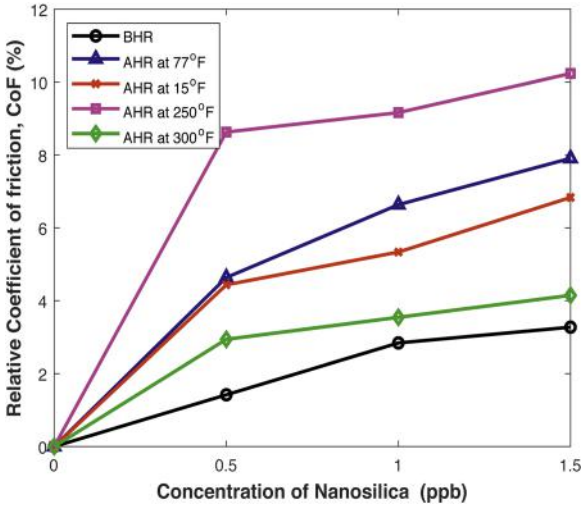

Fig. 16. Relative CoF reduction of 9 ppg OBM samples with and without nanosilica.

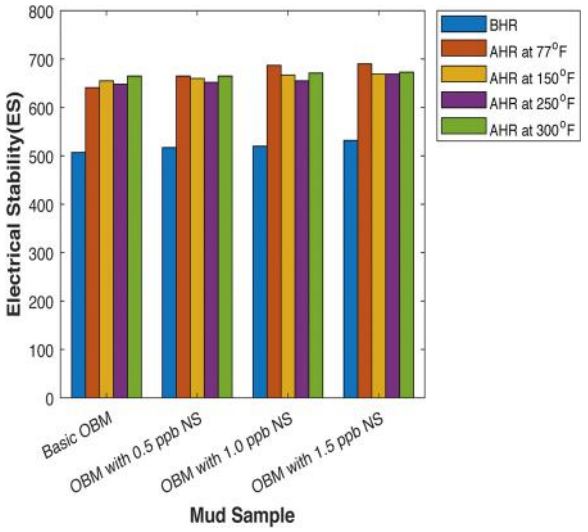

Fig. 17. ES of 12 ppg OBM samples with and without nanosilica.

at their respective temperature, ranging from 77 °F to 300 °F, for 16 h under a backpressure of 100 psi. The specification recommended by [56,57] for an ES test to indicate the stability of an emulsion is that the ES value be greater than or equal to 400 V.

All the OBM samples satisfy the ideal specifications suggested, exhibiting ES values greater than 400 V. Additionally, the ES values of the mud samples after aging are maintained above the desired value, which signifies that there is no degradation of the emulsifier within the systems.

Both the 9 ppg OBM and 12 ppg OBM samples display similar trends in terms of being able to maintain a stable emulsion throughout the study by satisfying the recommended specification. Moreover, the 12 ppg OBM samples have higher ES values than the 9 ppg OBM samples, which might occur because heavy muds contain less brine within their systems since the ES values signify the maximum voltage that an OBM can sustain before it starts to conduct current [10,62].

3.1.10. PV of 12 ppg OBM samples with and without nanosilica

Fig. 18 displays the PVs of the 12 ppg OBM samples with and without nanosilica at concentrations of 0.5 ppb to 1.5 ppb both before and after aging at a temperature ranging from 77 °F to 300 °F. The recommended range suggested by [56,57] is from 10 to 60 cp for any

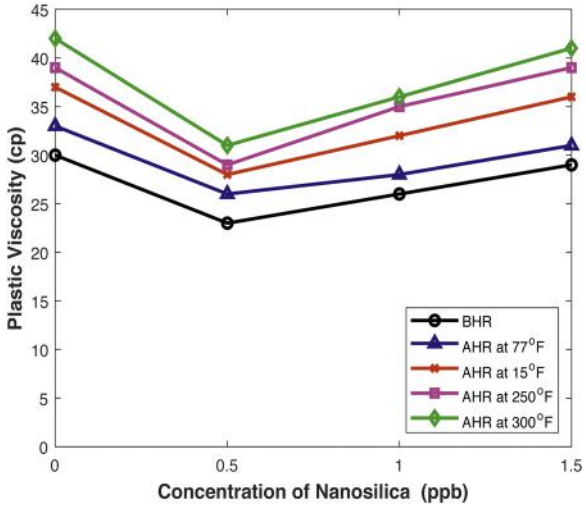

Fig. 18. PV of 12 ppg OBM samples with and without nanosilica.

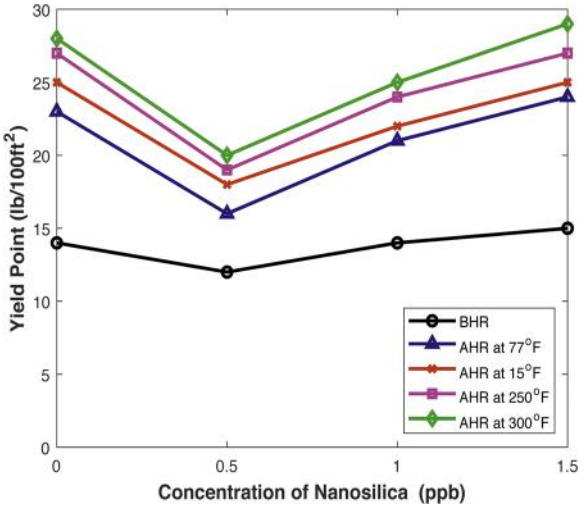

Fig. 19. YP of 12 ppg OBM samples with and without nanosilica.

heavy mud sample.

Referring to Fig. 18, the usage of nanosilica in OBM samples reduces the PVs of each set of samples relative to the basic mud, both before and after aging. The greatest reduction in the PV is observed when 0.5 ppb nanosilica is used for every set of samples. Above 0.5 ppb, a further increase in the nanosilica concentration does not reduce the PV further; instead, the use of a higher nanosilica concentration results in a smaller PV reduction, making the PVs of these nano-muds closer to the basic mud's PV.

Before aging, when 0.5 ppb, 1.0 ppb and 1.5 ppb nanosilica is used as the additive, the PV of the basic mud is reduced from 30 cp to 23 cp, 26 cp and 29 cp, respectively. After aging at 77 °F, the 0.5 ppb, 1.0 ppb and 1.5 ppb nanosilica-enhanced muds exhibit reductions in the PV compared to the basic mud from 30 cp to 21 cp, 21 cp and 25 cp, respectively.

Reductions in the PVs from that of the basic mud of 34 cp to 24 cp, 27 cp and 32 cp are observed for the OBM samples containing 0.5 ppb, 1.0 ppb and 1.5 ppb nanosilica, respectively, aged at 150 °F. When the OBM samples have been aged at 250 °F, the samples with 0.5 ppb, 1.0 ppb and 1.5 ppb nanosilica exhibit reduced PVs compared to the value of 35 cp for the basic mud of 25 cp, 28 cp and 33 cp, respectively. A similar trend occurs after the samples are aged at 300 °F, where reductions in the basic mud PV from 36 cp to 26 cp, 26 cp and 34 cp occur when the muds contains 0.5 ppb, 1.0 ppb and 1.5 ppb nanosilica, respectively.

As for the effect of the mud weight on the PV, the 12 ppg OBM samples generally have higher PV values than those of the 9 ppg OBM samples. This increase occurs because heavy mud has a higher solid content than normal mud weight samples [91], and a higher solid content often results in a higher PV [15].

3.1.11. YP of 12 ppg OBM samples with and without nanosilica

Fig. 19 displays the YP of the 12 ppg OBM samples with and without nanosilica both before and after aging. The ideal range of YP recommended by previous researchers [56,57] is 2.5–20 lb/100 sq ft for a heavy OBM mud.

Fig. 19 shows a pattern in which the YP of the OBM samples decreases when nanosilica is added as the mud additive. The greatest decrease of YP can be noted when the nanosilica concentration is 0.5 ppb both before and after aging. A further increase of the concentration above 0.5 ppb does not decrease the YP value further but instead results in a smaller reduction, bringing the YP value closer to that of the basic mud. Since a higher YP value will result in flocculation, a relatively moderate YP within the range is desired so that the mud does not flocculate but is strong enough to hold the drill cuttings.

Before aging, all the mud samples are within the suggested range of the ideal YP, with values of 14, 12, 14 and 15 lb/100 sq ft for the basic mud and 0.5, 1.0 and 1.5 ppb nanosilica-enhanced muds. However, after aging at 77 °F, only one mud sample is within the ideal YP range, the OBM sample with 0.5 ppb nanosilica. At this aging temperature, the basic mud has a value of 23 lb/100 sq ft, while the 1.0 ppb and 1.5 ppb nanosilica muds have YP values of 21 and 24 lb/100 sq ft, respectively.

When the samples are aged at 150 °F, similarly, only the 0.5 ppb nanosilica mud is within the suggested range, while the basic mud achieves a YP value of 25 lb/100 sq ft and the 1.0 ppb and 1.5 ppb nanosilica muds obtain YP values of 22 and 25 lb/100 sq ft, respectively.

For the OBM samples aged at a high temperature of 250 °F or 300 °F, only one sample from each case satisfies the ideal YP range, both of which are the 0.5 ppb nanosilica mud, with YP values of 19 and 20 lb/100 sq ft, respectively.

Comparing the 9 ppg and 12 ppg OBM samples, a difference in the patterns is observed. The YP of the 9 ppg OBM samples increases proportionally with increasing nanosilica concentration, which implies that the basic mud samples both before and after aging have the lowest YP value. In contrast, the YP values of the basic muds for the 12 ppg samples are usually the highest among all the muds in each condition. This difference in patterns occurs because of the difference in the solid content at each mud weight.

According to Salih [15], the YP is largely affected by the electrochemical attractive force and the frictional force between particles, and these two forces depend on the distance between solid particles; with an increase in the solid content within the same volume, the distance between solid particles is reduced, resulting in greater forces. In the basic mud, no nanosilica exists to rearrange the solid particles; hence, the greater forces directly result in higher YP values.

3.1.12. GS at 10 s of 12 ppg OBM samples with and without nanosilica

Fig. 20 shows the 10 s GSs of the 12 ppg OBM samples with and without nanosilica both before and after aging. The range of the 10 s GS recommended by previous researchers [56,57] is from 4 to 10 lb/100 sq ft.

From Fig. 20, under the conditions of before aging and low temperature aging in the temperature range from 77 °F to 150 °F, an increase in the nanosilica concentration generally increase the 10 s GS of the samples. However, only a few samples are in the ideal 10 s GS range, while the others exhibits undesirable 10 s GSs higher than the ideal range. The ideal samples include the basic mud sample, 0.5 ppb nanosilica OBM sample and 1.0 ppb nanosilica OBM sample before aging.

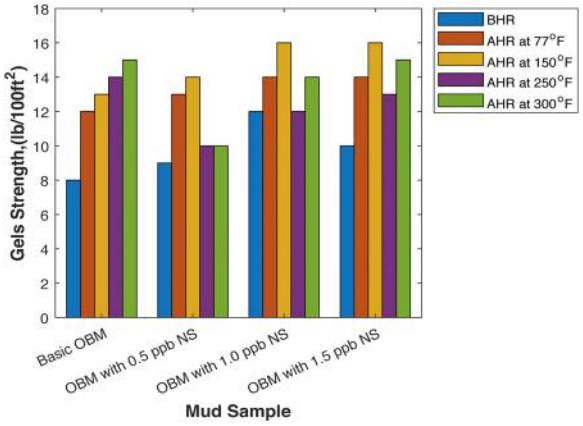

Fig. 20. GS at 10 s of 12 ppg OBM samples with and without nanosilica.

After aging at a high temperature range of 250 °F to 300 °F, the OBM samples exhibit a different pattern, in which the 10 s GSs of the basic muds are actually reduced by the addition of nanosilica. This decrease might be due to the solid particles in the basic mud samples undergoing degradation at higher temperature, while the mud samples with nanosilica have lower 10 s GSs because of the protective effect from the nanosilica [75]. The 0.5 ppb nanosilica OBM samples for each aging temperature condition are within the ideal range.

At lower temperature conditions (77 °F to 150 °F), an increase in the nanosilica concentration linearly increases the 10 s GS because of the increase in the solid content within the mud system. However, at higher temperature conditions (250 °F to 300 °F), the basic mud samples exhibit the highest values of the 10 s GS. The presence of nanosilica protects the mud particles, hence resulting in lower 10 s GSs. With increasing nanosilica concentration, the solid content and the 10 s GSs increase.

3.1.13. GS at 10 m of 12 ppg OBM samples with and without nanosilica

Fig. 21 demonstrates the 10 m GSs of 12 ppg OBM samples with and without nanosilica both before and after aging. The range of the 10 s GS recommended by previous researchers [56,57] is from 4 to 15 lb/100 sq ft.

Fig. 21 shows that the 10 m GS has a similar pattern to the 10 s GS. Before aging and after aging at low temperature, the 10 m GS exhibits an increase with the addition of nanosilica and with increasing nanosilica concentration. Unfortunately, only two samples are within the recommended specifications: the basic mud sample and the OBM sample with 0.5 ppb nanosilica before aging. After aging at a higher temperature ranging from 250 °F to 300 °F, a similar trend to that exhibited by the 10 s GS is observed because the basic mud samples generally have higher 10 m GS values, which may result from flocculation. Only one sample is within the ideal specification, the OBM sample with 0.5 ppb nanosilica aged at 300 °F.

Fig. 22 shows the comparison of the 10 s and 10 m GSs of each set of 12 ppg OBM samples before aging and after aging at their respective temperature. The aim of this comparison is to investigative if a particular OBM sample has an appreciable range of differences between its 10 s and 10 m GSs to ensure the formation of a progressive gel for cuttings suspension.

Although some of the 10 s and 10 m GSs are not within the ideal specifications, appreciable differences still exist between the 10 s and 10 m GSs of each sample. This result signifies that progressive gels are successfully formed, which is a very desirable property for any mud sample.

An increase in temperature generally increases the 10 s and 10 m GSs for a sample [92], as can be seen in both Figs. 20–22, in which the 10 s and 10 m GSs of the samples after aging at any temperature are higher than those of their respective samples before aging.

The effect of the mud weight on the 10 s and 10 m GSs of the OBM samples can also be investigated by comparing the results obtained for the 9 ppg OBM and 12 ppg OBM. Based on the comparison, OBM samples of higher mud weight have higher 10 s and 10 m GS values due to the higher amount of solid content present in the heavy mud system.

3.1.14. HPHT filtration of 12 ppg OBM samples with and without nanosilica

Fig. 23 shows the results of HPHT filtration conducted on the 12 ppg OBM samples with nanosilica concentration from 0.5 ppb to 1.5 ppb aged at a high temperature ranging from 250 °F to 300 °F. The ideal specification for an HPHT filtration test recommended by previous researchers [56,57] is that the filtrate volume be less than or equal to 10 cc after 30 min of testing.

In Fig. 23, a trend is observed in which, with the addition of nanosilica, the filtration volume tends to increase with increasing nanosilica concentration. Nevertheless, all the samples still fulfill the ideal specification of having an HPHT filtration loss of less 10 cc.

The OBM samples aged at 250 °F experience a greater fluid loss when a higher concentration of nanosilica is used as an additive. The basic mud sample only experiences a fluid loss of 2.0 cc, while the samples with 0.5 ppb, 1.0 ppb and 1.5 ppb nanosilica experience losses of 2.6 cc, 3.4 cc and 3.8 cc, respectively.

A similar pattern is observed for the samples aged at 300 °F, in which the basic mud sample has the lowest filtration loss value of only 3.2 cc, while the other samples with nanosilica have greater fluid loss compared to the basic mud. The 0.5 ppb, 1.0 ppb and 1.5 ppb nanosilica-enhanced muds experience fluid losses of 3.8 cc, 4.8 cc and 5.2 cc, respectively.

A comparison between the HPHT filtration losses of the 9 ppg and 12 ppg OBM samples is performed to study the impact of the mud weight on the fluid loss of the mud samples. From the comparison, the filtration losses experienced by the 12 ppg OBM samples are generally higher than those by the 9 ppg OBM samples. This higher loss occurs because the 12 ppg OBM samples contain a higher solid content and have higher PV values compared to the 9 ppg samples. The comparison results verify the theory of Salih [15] that the flocculation effect is more severe in samples with a higher solid content, as flocculation creates a pathway that favors a higher fluid loss.

3.1.15. Mud cake thickness of 12 ppg OBM samples with and without nanosilica

Fig. 24 shows the mud cakes thicknesses of the 12 ppg OBM samples tested in the HPHT filtration test, which were aged at the temperatures of 250 °F and 300 °F.

From Fig. 24, the thickness of the mud cakes obtained is directly proportional to the filtration loss experienced by the OBM samples. The thickest mud cakes of 4/32 inches are obtained for the samples aged at 300 °F with 1.0 ppb and 1.5 ppb nanosilica concentrations. Meanwhile the thinnest mud cake of only 2/32 inches is obtained for the basic mud

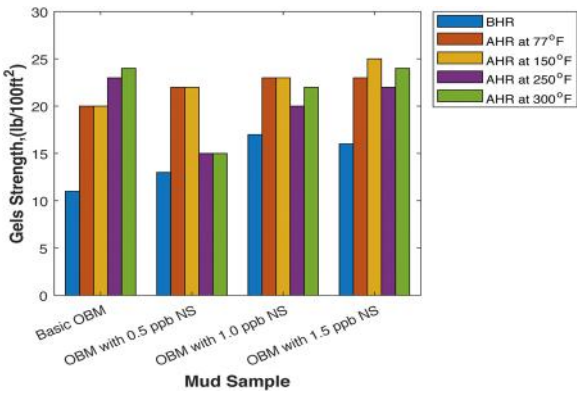

Fig. 21. GS at 10 m of 12 ppg OBM samples with and without nanosilica.

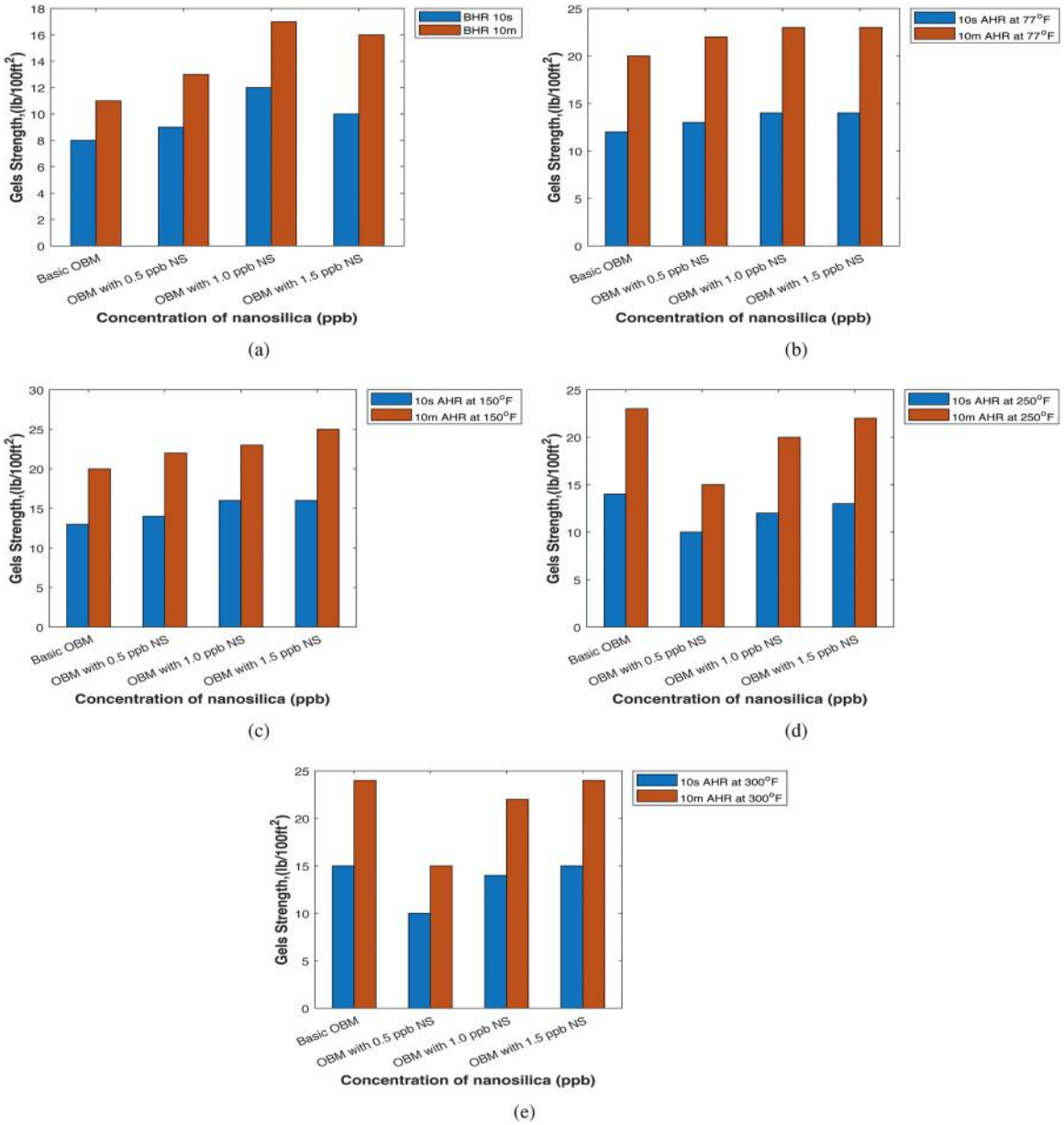

Fig. 22. Comparison of 10 s and 10 m GSs of 12 ppg OBM samples with different aging temperatures: (a) before aging, (b) after aging at 77 °F, (c) after aging at 150 °F, (d) after aging at 250 °F and (e) after aging at 300 °F.

sample aged at 250 °F.

Increases in the temperature and mud weight increase the filtration loss of the OBM samples tested; hence, the mud cake thickness is indirectly affected since it is only directly impacted by the fluid loss volume of the studied samples.

3.1.16. Lubricity of 12 ppg OBM samples with and without nanosilica

Fig. 25 demonstrates the CoF values of the 12 ppg OBM samples with and without nanosilica both before and after aging, while Fig. 26 displays the CoF reductions of every nanosilica-enhanced sample relative to its basic mud at the respective condition.

From Fig. 25, a pattern of decreasing CoF with increasing nanosilica concentration is obtained, both before aging and after aging. This result implies that the 1.5 ppb nanosilica muds can provide the lowest CoF values regardless of the condition.

For instance, with the usage of 1.5 ppb nanosilica, before aging, a 2.2% relative CoF reduction is obtained. The highest relative reduction among all the samples is exhibited by the 1.5 ppb nano-mud post-77 °F aging, with a relative CoF reduction of up to 8%. When the OBM samples are aged at 150 °F, 250 °F and 300 °F, the 1.5 ppb nanosilica muds exhibit relative CoF reductions of 5.2%, 6.9% and 7.2%, respectively.

3.1.17. Rheological modeling of OBM samples with and without nanosilica

Rheological modeling is often conducted to investigate which rheological model best describes the selected drilling fluid sample A few rheological models are obtained, and the shear stress and shear rate measurements of the studied mud samples are compared with the parameters generated by all the rheological models. Trend lines are generated from both the studied mud samples and rheological models, and comparison and matching of the lines are performed in order to determine which law of fluids the mud samples follow. The deviation error is used to help identify the correct rheological model.

The selected samples for this rheological modeling are the basic mud of each mud weight as well as the mud samples that contain 0.5 ppb nanosilica because, overall, the 0.5 ppb nanosilica OBM

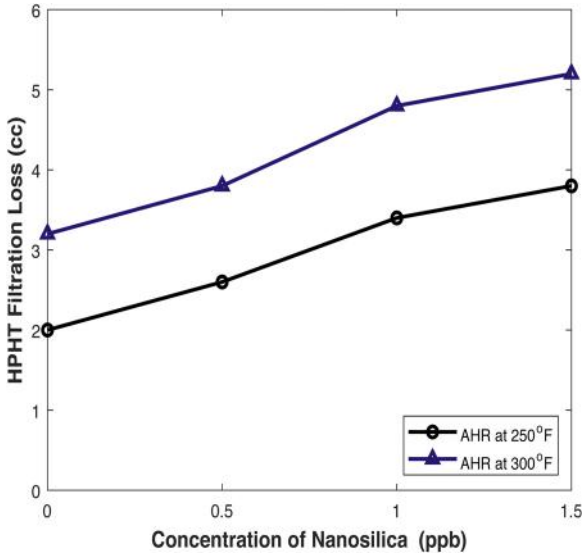

Fig. 23. HPHT filtration of 12 ppg OBM samples with and without nanosilica.

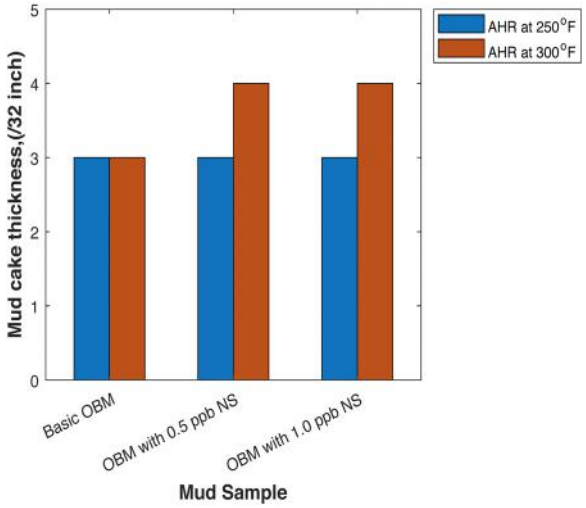

Fig. 24. Mud cake thickness of 12 ppg OBM samples with and without nanosilica.

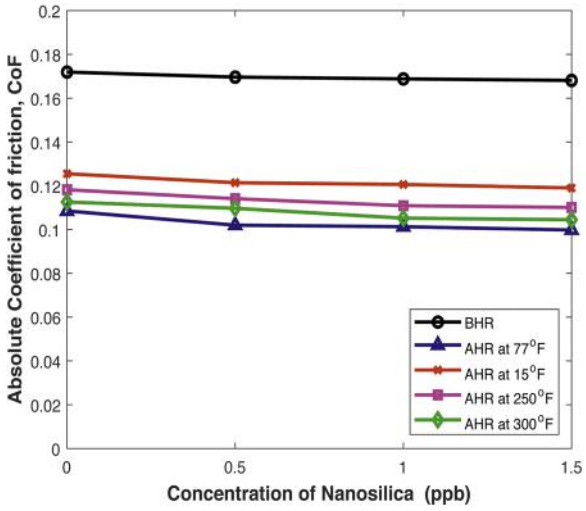

Fig. 25. CoF of 12 ppg OBM samples with and without nanosilica.

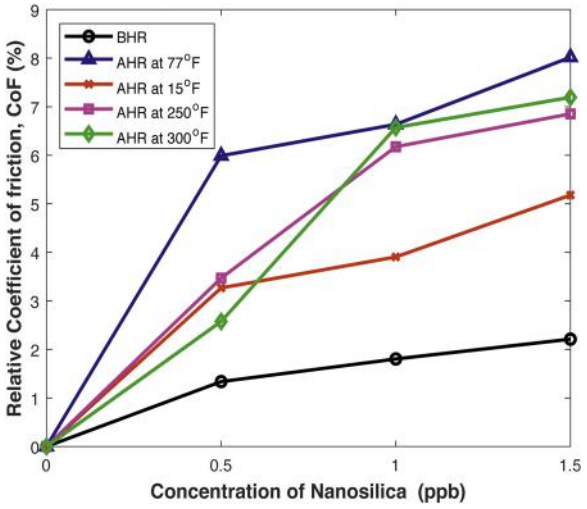

Fig. 26. Relative CoF reduction of 12 ppg OBM samples with and without nanosilica.

samples have performed optimally in terms of almost all the rheological properties investigated. The types of rheological models investigated are the Newtonian [9], Bingham [93], Herschel–Bulkley [94] and Ostwald power law models [95].

The results obtained from the modeling of the 9 ppg OBM basic mud sample are tabulated and plotted in Table 8 and Fig. 27, respectively.

From Fig. 27, the largest deviation is observed for the Newtonian model, with an error of 9.53%. Additionally, the trend line for the 9 ppg OBM basic mud most closely matches that of the Herschel–Bulkley model, which is confirmed by the deviation error of only 1.16%. Hence, the Herschel–Bulkley [94] model is the most suitable model to describe the 9 ppg basic OBM sample.

The modeling results of the 9 ppg OBM sample with 0.5 ppb nanosilica are tabulated and plotted in Table 9 and Fig. 28, respectively.

As illustrated in Fig. 28 and Table 9, the highest deviation is observed for the Ostwald model [95], with a deviation error of nearly 7%, while the other models exhibit deviation errors of greater than 3% except for the Herschel–Bulkley [94] model. The error of this model is only 0.84%, making it the most appropriate rheological model for the 9 ppg OBM sample with 0.5 ppb nanosilica.

The modeling results of the 12 ppg OBM basic mud are tabulated and plotted in Table 10 and Fig. 29, respectively.

As demonstrated in Fig. 29, the Newtonian model is undefined in the modeling test of the 12 ppg OBM basic mud sample, which is in line with the theory that drilling fluids do not behave like Newtonian fluids (Forthun [96]). According to the figure, the trend line of the mud sample matches the lines of both the Bingham plastic model [93] and Herschel–Bulkley model [94]; however, the deviation error percentage from Table 10 indicates that the 12 ppg basic mud sample behaves according to the Herschel–Bulkley model [94], with an error value of only 1%.

The modeling results of the 12 ppg OBM containing 0.5 ppb nanosilica are tabulated and plotted in Table 11 and Fig. 30, respectively.

A similar pattern is observed in Fig. 30: the Newtonian model is also undefined, and the trend line of the 12 ppg OBM with 0.5 ppb nanosilica again falls between the trend lines of the Bingham plastic [93] and Herschel–Bulkley [94] models. Nevertheless, the deviation error from Table 11 indicates that the most accurate model to describe the 12 ppg OBM with 0.5 ppb nanosilica is the Herschel–Bulkley [94] model, with an error value of only 1.1%.

3.2. Rheological properties of WBM samples

The rheological properties investigated for WBM are the PV,

Table 8
Modelled equations for 9 ppg OBM basic mud.

Model	Equation	Parameters				Error (%)
		τ_o, τ_y	k	n	μ_p, μ	
Newtonian [9]	$\tau = 0.0193\gamma$				0.0193	9.53
Bingham [93]	$\tau = 0.0112 \cdot \gamma + 1.2286$	1.2286			0.0112	2.94
HerschelBulkley [94]	$\tau = 1.0869 + 0.0426(\cdot\gamma^{0.7483})$	1.0869	0.0426	0.7483		1.16
OstwaldPower Law [95]	$\tau = 1 \cdot \gamma^{0.1988}$		1	0.1988	3.81	

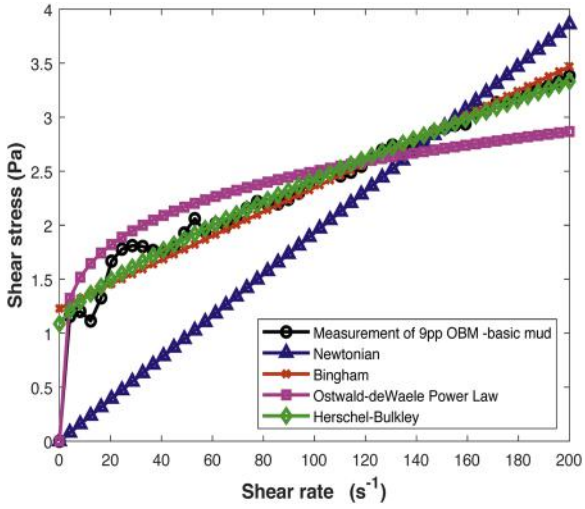

Fig. 27. Rheological modeling of 9 ppg OBM basic mud.

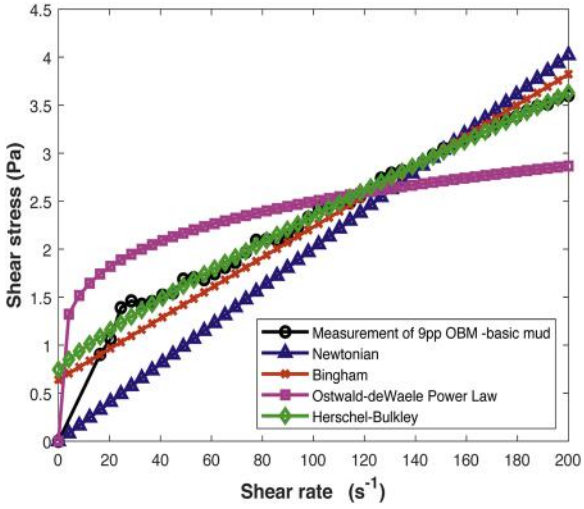

Fig. 28. Rheological modeling of 9 ppg OBM with 0.5 ppb nanosilica.

apparent viscosity, YP, gel strength of each mud sample at both 10 s and 10 min, API filtration and HPHT filtration. Mud cake thickness and lubricity tests are also conducted, and rheological models are obtained.

Since WBMs of two mud weights are studied, two different guidelines, i.e., Tables 12 and 13, are obtained from SCOMI Oil Tools [97] as benchmark specifications to evaluate the performance of all the formulated WBM samples.

3.2.1. PV of 9 ppg WBM samples with and without nanosilica

Fig. 31 represents the PVs of the 9 ppg WBM samples with and without nanosilica before and after aging at their respective aging temperatures. The recommended range for PVs is less than or equal to 30 cp at both low and high temperature conditions.

As shown in Fig. 31, almost all the samples satisfy the ideal PV for a mud except the basic mud sample aged at 150 °F. The addition of nanosilica to 9 ppg WBM decreases the PV values, and the reduction of PV increases as the nanosilica concentration increases up to 1.0 ppb. This trend is the same for all conditions, both before and after hot rolling. After the nanosilica concentration reaches 1.0 ppb, a further increase of the concentration does not further increase the reduction but instead brings the PV value closer to that of the basic mud for each condition.

The trend of the impact of nanosilica can be explained by the fact that the nanosilica particles are well dispersed around and between the bentonite platelets and cation exchange occurs in which the negatively charged nanosilica neutralizes the positive charge on the bentonite surfaces, hence converting them to negatively charged bentonite platelets overall. This negative charge strengthens the repulsive force among bentonite platelets and leads to an increase in the distance among all the bentonite particles; as a result, less friction is experienced [15]. Additionally, nanosilica acts as ball bearings by lubricating the surface of the bentonite particles, thus ensuring the decrease in the frictional force and thereby giving rise to a reduction of the PV.

For example, before hot rolling, the PV value of the basic mud is reduced from 15 cp to 13 cp with the usage of 1.0 ppb nanosilica. Moreover, after hot rolling at the temperatures of 77 °F, 150 °F, 250 °F and 300 °F, the addition of 1.0 ppb nanosilica reduces the PV relative to that of the respective WBM basic mud sample, from 28 to 15 cp, from 31 to 21 cp, from 22 to 18 cp and from 22 cp to 15 cp, respectively.

On the other hand, an increase in the aging temperature clearly results in a generally lower PV value compared to those obtained for the WBM samples that have undergone low temperature aging. This result occurs because at a higher temperature, the kinetic energy of the particles, especially the bentonite particles, is higher; hence, they tend to move faster and more vigorously [63], which leads to a large increase in the distance among the bentonite particles and a lower PV.

The PV should be kept low, as this favors a higher ROP and better

Table 9
Modelled equations for 9 ppg OBM with 0.5 ppb of nanosilica.

Model	Equation	Parameters				Error (%)
		τ_o, τ_y	k	n	μ_p, μ	
Newtonian [9]	$\tau = 0.0201\gamma$				0.0201	5.98
Bingham [93]	$\tau = 0.0159 \cdot \gamma + 0.642$	0.642			0.0159	3.69
HerschelBulkley [94]	$\tau = 0.7458 + 0.0319(\cdot\gamma^{0.8502})$	0.7458	0.0319	0.8502		0.84
OstwaldPower Law [95]	$\tau = 1 \cdot \gamma^{0.1948}$		1	0.1948	6.70	

Table 10
Modelled equations for 12 ppg OBM basic mud.

Model	Equation	Parameters				Error (%)
		τ_o, τ_y	k	n	μ_p, μ	
Newtonian [9]	Undefined					
Bingham [93]	$\tau = 0.0239 \cdot \gamma + 3.3252$	3.3252			0.0239	7.17
HerschelBulkley [94]	$\tau = 3.7762 + 0.0109(\cdot\gamma^{0.1.1261})$	3.7762	0.0109	1.1261		1.00
OstwaldPower Law [95]	$\tau = 2.0544 \cdot \gamma^{0.2339}$		2.0544	0.2339	6.53	

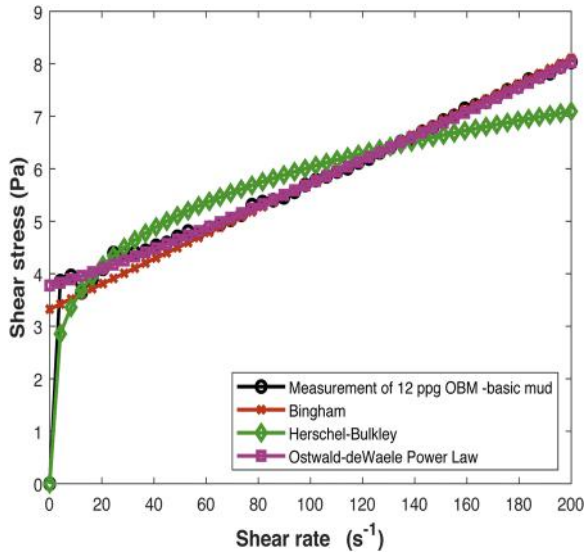

Fig. 29. Rheological modeling of 12 ppg OBM basic mud.

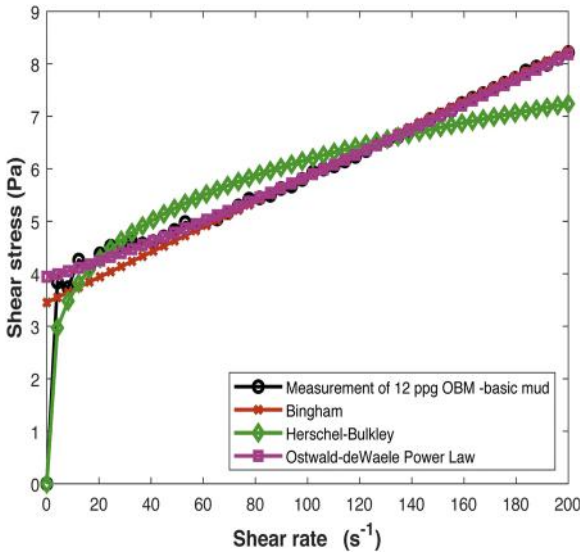

Fig. 30. Rheological modeling of 12 ppg OBM with 0.5 ppb nanosilica.

cooling and lubrication of the downhole equipment, saves energy in mud circulation and reduces the chances of mud circulation loss to the formation fractures formed by an excessive equivalent circulation density of the mud.

3.2.2. YP of 9 ppg WBM samples with and without nanosilica

Fig. 32 represents the YPs of the 9 ppg WBM samples with and without nanosilica before and after hot rolling at their respective aging temperature. The ideal YP suggested by Scomi Oil Tools [97] is below 50 lb/100 sq ft for low temperature conditions and between 10 and 25 lb/100 sq ft for high temperature conditions.

As observed from Fig. 32, at the low temperature conditions, almost all YP values of the samples are within the recommended range, except for those of the basic mud samples hot rolled at 77 °F and 150 °F, which are 55 lb/100 sq ft and 52 lb/100 sq ft, respectively. On the other hand, the samples aged at high temperature conditions show a good performance by satisfying the ideal range.

With the addition of nanosilica, the YP of WBM decreases with increasing nanosilica concentration up to 1.0 ppb; at this concentration, all the WBM samples exhibit the lowest YP value for their respective condition. A further increase of the nanosilica concentration only brings the YP value closer to that of the respective basic mud.

The YP is closely related to the PV because the YP largely depends on both the electrochemical attractive and frictional forces, which are easily affected by the distance of the bentonite particles [15]. Hence, since the usage of nanosilica increases the distance among the bentonite particles, a lower PV is obtained, as is a lower YP.

Since the YP of a WBM is directly associated with its PV, the effect of temperature on the YP is similar to that on the PV.

Table 12
Recommended rheological properties for WBM at low temperature conditions (SCOMI Oil Tools,2017 [97]).

Rheological property	Specification
Plastic viscosity, cp	< 30
Yield point, lb/100 sq. ft	< 50
Gel strength (10 s)	< 15
Gel strength (10 min)	< 35
API fluid loss, cc/30 min	< 15
API mud cake thickness, /32 inch	< 3

Table 11
Modelled equations for 12 ppg OBM with 0.5 ppb of nanosilica.

Model	Equation	Parameters				Error (%)
		τ_o, τ_y	k	n	μ_p, μ	
Newtonian [9]	Undefined					
Bingham [93]	$\tau = 0.024 \cdot \gamma + 3.4522$	3.4522			0.024	7.46
HerschelBulkley [94]	$\tau = 3.9418 + 0.0096(\cdot\gamma^{1.1497})$	3.9418	0.0096	1.1497		1.10
OstwaldPower Law [95]	$\tau = 2.1514 \cdot \gamma^{0.229}$		2.1514	0.229	6.54	

Table 13
Recommended rheological properties for WBM at high temperature conditions (SCOMI Oil Tools [97]).

Rheological property	Specification
Plastic viscosity, cp	< 30
Yield point, lb/100 sq. ft	10–25
Gel strength (10 s)	< 15
Gel strength (10 min)	< 35
API fluid loss, cc/30 min	< 15
API mud cake thickness, /32 inch	< 3
HPHT fluid loss, cc/30 min	25
HPHT mud cake thickness, /32 inch	< 10

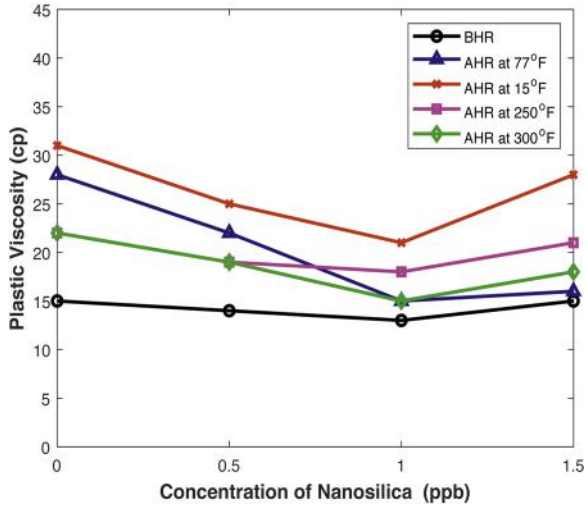

Fig. 31. PV of 9 ppg WBM samples with and without nanosilica.

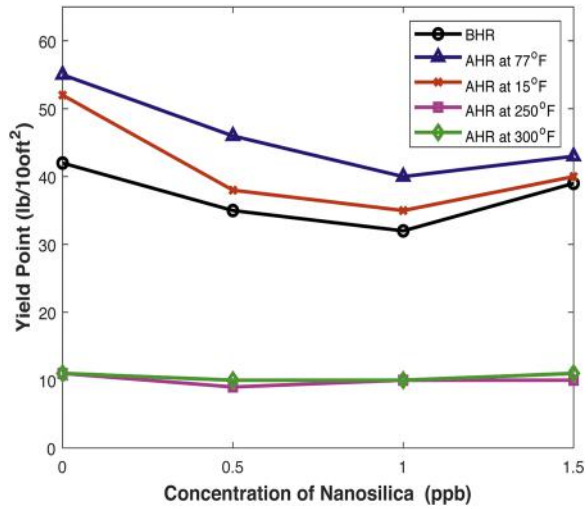

Fig. 32. YP of 9 ppg WBM samples with and without nanosilica.

3.2.3. Gel strength at 10 s of 9 ppg WBM samples with and without nanosilica

Fig. 33 represents the 10 s GSs of the 9 ppg WBM samples with and without nanosilica before and after hot rolling at a temperature ranging from 77 °F to 300 °F. The suggested range for the 10 s GS of a WBM is less than or equal to 15 lb/100 sq ft for the samples before aging, the samples aged at low temperature conditions and those that have undergone hot rolling at high temperature conditions.

Referring to Fig. 33, of all the samples, only two are within the range of the suggested specifications for the 10 s GS: the WBM samples containing 1.0 and 1.5 ppb nanosilica hot rolled at 150 °F.

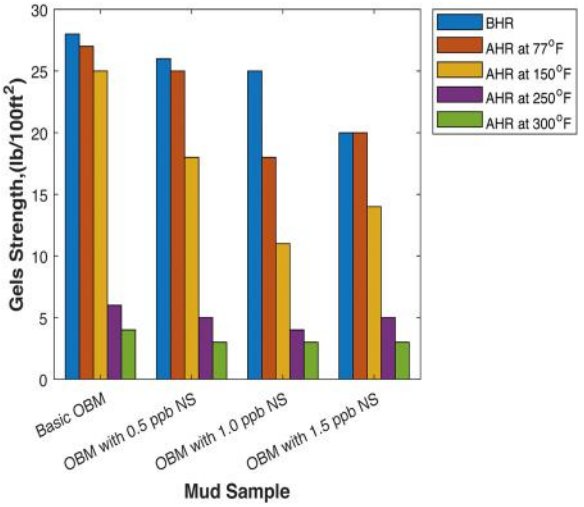

Fig. 33. GS at 10 s of 9 ppg WBM samples with and without nanosilica.

Conversely, all the WBMs that have undergone hot rolling at high temperature are within the recommended range. An increase in temperature extensively decreases the 10 s GS, as the gel strength is also a parameter that depends on the PV of a mud sample.

Generally, an increase in the nanosilica concentration decreases the 10 s GS of the WBM, as the usage of nanosilica can enable the development of a fragile gel [15]. A fragile gel is required, as it enables the mud system to be effortlessly resumed and to suspend cuttings as well as enables the easy removal of cuttings at the shale shakers.

3.2.4. Gel strength at 10 m of 9 ppg WBM samples with and without nanosilica

Fig. 34 displays the 10 m GSs of the 9 ppg WBM samples with and without nanosilica both before and after aging. The ideal range for the 10 m GS of a WBM sample is less than or equal to 35 lb/100 sq ft.

As demonstrated in Fig. 34, only two samples for the low temperature conditions manage to satisfy the recommended range: the samples with 1.0 ppb and 1.5 ppb nanosilica aged at 150 °F. Fortunately, all the samples that have undergone hot rolling at 250 °F and 300 °F successfully fulfill the specifications. A fragile gel is desired for the instantaneous resumption of mud circulation. The lowest 10 m GS is obtained when 1.0 ppb nanosilica is used. However, a further increase in the nanosilica concentration results in an increase in the 10 m GS. This result occurs because an increase of the nanosilica concentration

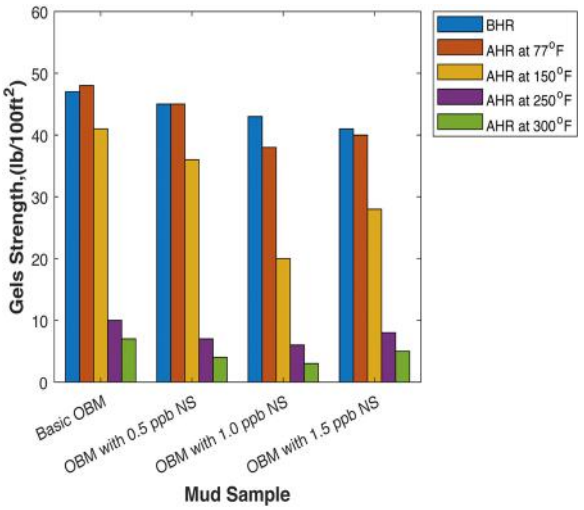

Fig. 34. GS at 10 m of 9 ppg WBM samples with and without nanosilica.

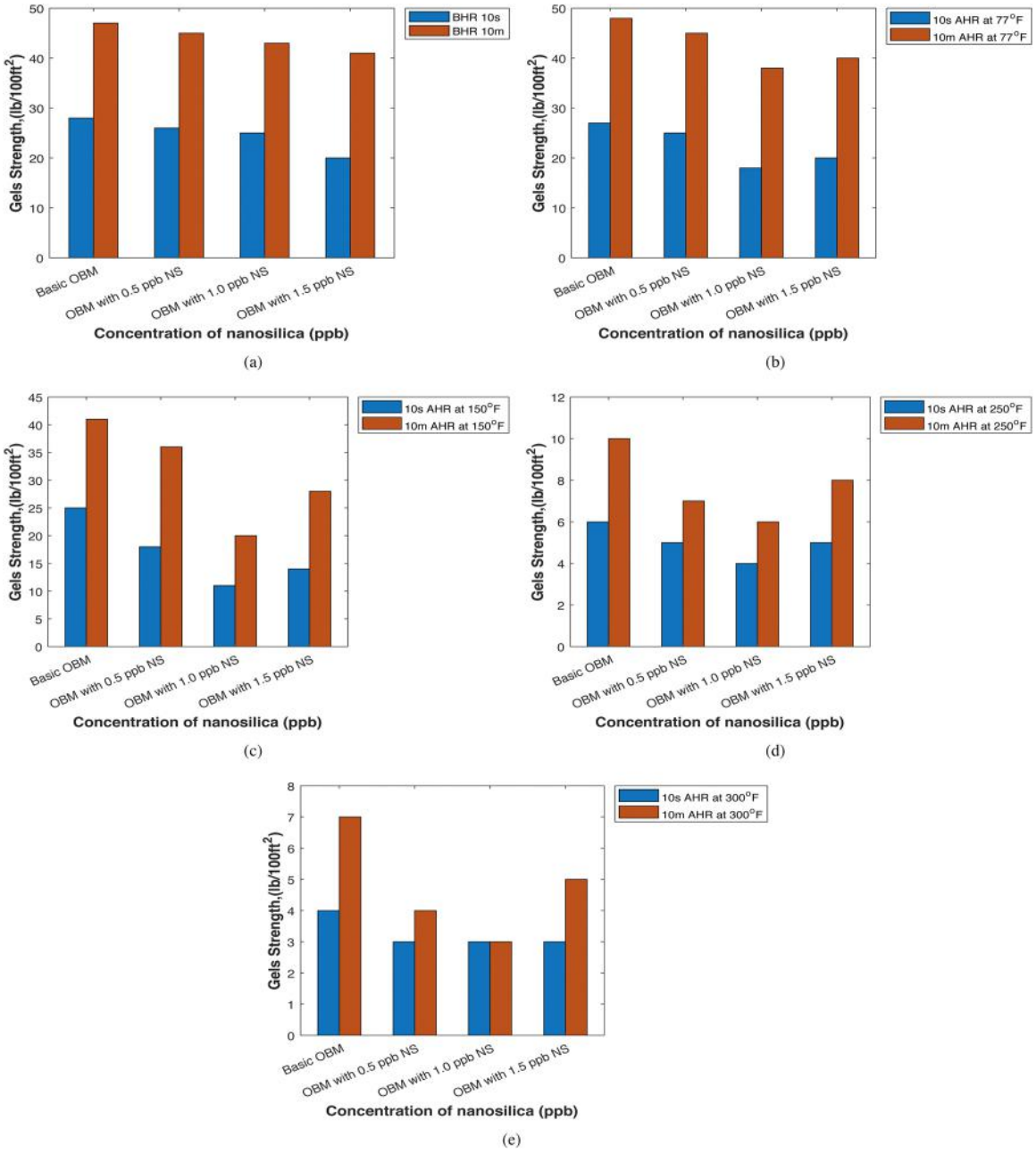

Fig. 35. Comparison of 10 s and 10 m GSs of 9 ppg WBM samples aged at different temperatures: (a) before aging, (b) after aging at 77 °F, (c) after aging at 150 °F, (d) after aging at 250 °F and (e) after aging at 300 °F.

beyond the optimum concentration will result in nanosilica agglomeration.

Fig. 35 shows the comparison of the 10 s and 10 m GSs of each sample for each condition in order to inspect the formation of progressive gels, which are fairly vital in ensuring the ability to instantaneously resume mud circulation, suspend cuttings and prevent sagging of barite.

Fortunately, almost all the WBM samples manage to form a progressive gel by having an appreciable range between the 10 s and 10 m GSs, except for the mud samples aged at 300 °F that contain 0.5 ppb and 1.0 ppb nanosilica. These two samples developed a low-flat gel instead. A low-flat gel is undesirable, as it would not be able to provide enough strength to suspend cuttings and even result in sagging of barite.

3.2.5. API filtration of 9 ppg WBM samples with and without nanosilica

Fig. 36 illustrates the API filtration of 9 ppg WBM samples with and without nanosilica. This filtration test is conducted using an LPLT filter press in order to test the filtration losses of all mud samples before and after aging. The ideal specification is that the fluid loss of a WBM be less than or equal to 15 cc for 30 min.

Referring to Fig. 36, a pattern can be noted in which almost all the samples experience a greater fluid loss with the addition of nanosilica, as the fluid loss increases with increasing nanosilica concentration. All the samples exhibit the same trend except for those tested before hot rolling, as in this condition, the fluid losses experienced by the WBM samples are inversely proportional to an increase of the nanosilica concentration [73,84].

All the samples for the conditions of before hot rolling and after aging at 77 °F and 150 °F have fluid losses within the recommended range. Only one samples from the condition of after aging at 250 °F satisfies the specifications suggested: the basic mud sample.

The reason for the increase of fluid losses with increasing nanosilica

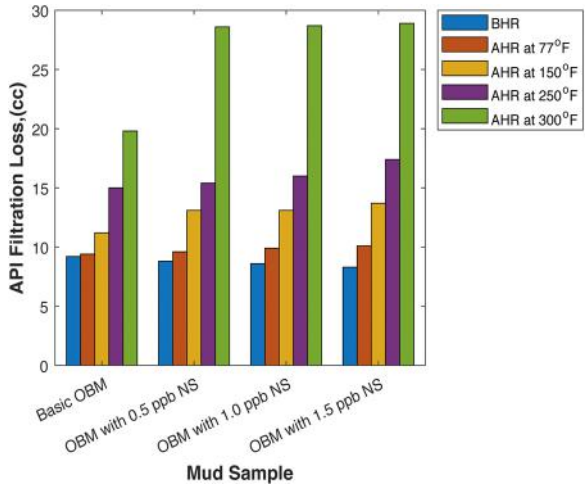

Fig. 36. API filtration of 9 ppg WBM with and without nanosilica.

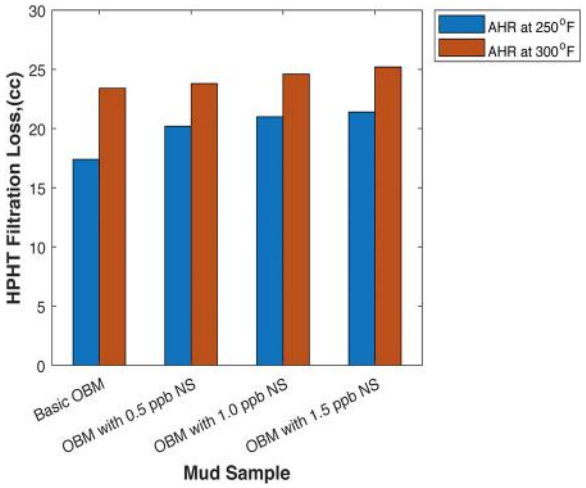

Fig. 38. HPHT filtration of 9 ppg WBM with and without nanosilica.

concentration is that nanosilica usage increases the distance among bentonite particles [15], which prevents the packing of solid particles on the filter paper to form an impermeable cake to reduce fluid loss.

As mentioned by Li et al. [98], the surfaces of nanosilica are composed of a huge number of hydrophilic groups, and if nanosilica particles pack on a filter paper, they will bind the free water through a surface wetting action. However, this phenomenon does not occur in our case because, as claimed by Salih [15], the nanosilica particles are distributed among and around the bentonite platelets, increasing the distance among the platelets due to surface repulsion; this mechanism thus hinders the packing of solid particles to form an impermeable mud cake to prevent the loss of fluid. Mud cakes formed for the high temperature samples are also not compact due to the dispersion of the bentonite particles.

3.2.6. API mud cake thickness of 9 ppg WBM samples with and without nanosilica

Fig. 37 demonstrates the API mud cake thicknesses of the 9 ppg WBM samples with and without nanosilica obtained from the API filtration test. The recommended specification of SCOMI [97] Oil Tools for an API mud cake is that its thickness should be less than or equal to 3/32 inches.

According to Fig. 37, a pattern can be found in which the mud cake thickness is closely associated with the API fluid loss experienced by each sample. All samples for low temperature conditions are successfully within the recommended range, while only two samples for the high temperature conditions are within the range: the basic mud and 0.5 ppb nanosilica samples aged at 250 °F. The samples that experienced greater fluid losses have rather thick mud cakes, as the failure of the formation of a thin impermeable cake leads to greater fluid loss.

3.2.7. HPHT filtration of 9 ppg WBM samples with and without nanosilica

Fig. 38 illustrates the HPHT filtration of the 9 ppg WBM samples with and without nanosilica only for the samples that have been aged at a high temperature ranging from 250 °F to 300 °F. The recommended value of the HPHT fluid loss is that it be less than or equal to 25 cc for 30 min of filtration.

The trend observed from Fig. 38 is similar to that for API filtration, as an increase in the nanosilica concentration increases the HPHT fluid loss. Despite this trend, almost all fluid losses of the samples are below 25 cc after 30 min of HPHT filtration, except for that of the 1.5 ppb nanosilica WBM aged at 300 °F, with a value of 25.2 cc. However, the extra fluid loss of 0.2 cc should be tolerable due to its insignificance.

3.2.8. HPHT mud cake thickness of 9 ppg WBM samples with and without nanosilica

Fig. 39 portrays the HPHT mud cake thicknesses of the 9 ppg WBM samples with and without nanosilica after the samples have undergone the HPHT filtration test. The ideal range recommended for an HPHT mud cake is that its thickness be less than or equal to 10/32 inches.

Referring to Fig. 39, similar to the mud cakes obtained from the API filtration test, the thicknesses of the HPHT mud cakes are directly

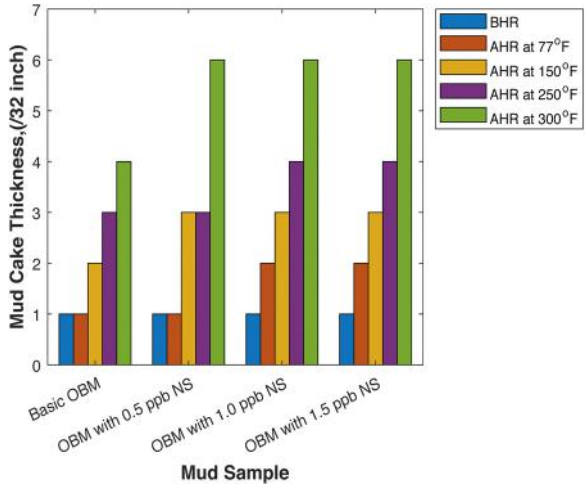

Fig. 37. API mud cake thickness of 9 ppg WBM with and without nanosilica.

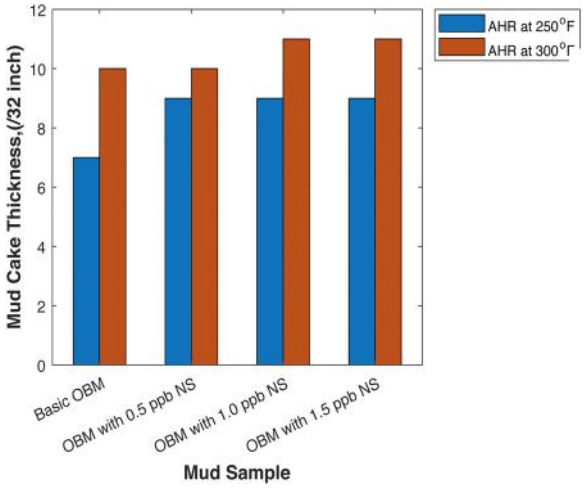

Fig. 39. HPHT mud cake thickness of 9 ppg WBM with and without nanosilica.

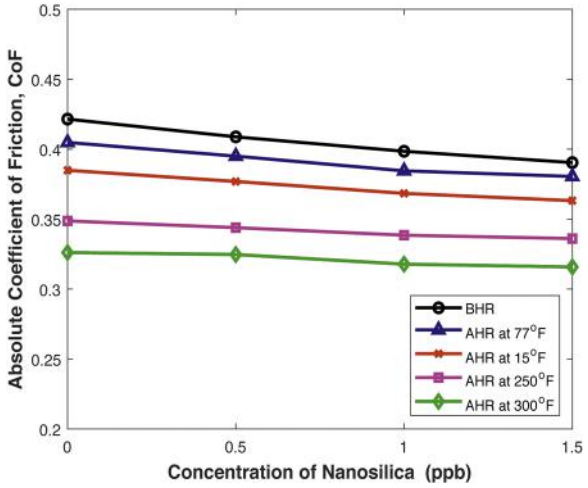

Fig. 40. CoF of 9 ppg WBM samples with and without nanosilica.

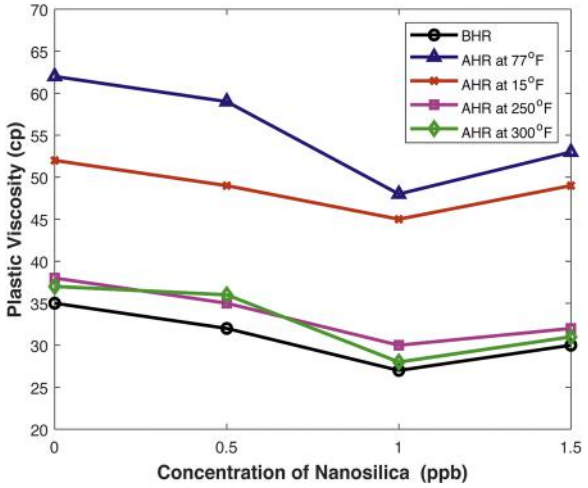

Fig. 42. PV of 12 ppg WBM samples with and without nanosilica.

impacted by the HPHT filtration volume loss. Only two samples do not fulfill the recommended specifications, the 1.0 and 1.5 ppb nanosilica samples, as they both have the same HPHT fluid losses of 11 cc after 30 min of filtration.

3.2.9. Lubricity of 9 ppg WBM samples with and without nanosilica

Fig. 40 demonstrates the CoF values of the 9 ppg WBM samples with and without nanosilica both before and after aging, while Fig. 41 displays the reduction of the CoF of every nanosilica-enhanced sample relative to its basic mud at the respective condition.

According to Fig. 41, an obvious trend can be stated, that an increase in the nanosilica concentration increases the reduction of the CoF. This result occurs because the dispersion of nanosilica enables it to act as ball bearings in lubricating the surface of the equipment, resulting in the reduction of the CoF [15,89].

The highest relative CoF reduction occurs when the nanosilica concentration for a particular condition is the highest. The relative CoF reduction is the reduction in the CoF of a nano-mud sample relative to the CoF of its basic mud counterpart. Before aging and after aging at 77 °F, 150 °F, 250 °F and 300 °F, the 1.5 ppb nanosilica WBM samples exhibit relative reductions of 7.4%, 6%, 5.6%, 3.6% and 3.2%.

Interestingly, different from the OBM samples, the WBM samples' lubricity is impacted by temperature. As seen from Fig. 41, the relative CoF reduction of each set of WBMs is higher for lower temperature conditions. Alshubbar et al. [89] mentioned that friction is reduced

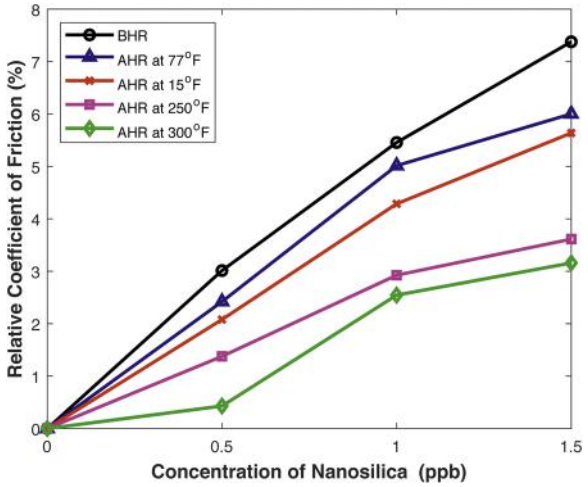

Fig. 41. Relative CoF reduction of 9 ppg WBM samples with and without nanosilica.

when nanosilica forms a thin film on the metal surface of the lubricity equipment, achieving a better lubricity. Meanwhile, Salih [15] stated that nanosilica particles are attached to bentonite particles in the mud systems, and the particles repel each other due to repulsion forces. At higher temperatures, according to kinetic theory [63], the bentonite particles are even further apart, which in turn leads to the inefficiency of nanosilica in forming a thin film that can cover the entire metal surface. Increasing the nanosilica concentration at a particular temperature condition enables more nanosilica to participate in the formation of a thin film lubricating the metal surface of the lubricity equipment.

3.2.10. PV of 12 ppg WBM samples with and without nanosilica

Fig. 42 displays the PVs obtained for the 12 ppg WBM samples with and without nanosilica both before and after aging at their respective aging temperature. The ideal range proposed by SCOMI [97] Oil Tools is that the PV of a WBM sample be less than or equal to 30 cp.

According to Fig. 42, only three samples satisfy the recommended specifications: the samples containing 1.0 ppb nanosilica before aging and after aging at 250 °F and 300 °F, with PV values of 27, 30 and 28 cp.

The effects of temperature and nanosilica concentration on the PV of the 12 ppg WBM are similar to those on the 9 ppg WBM, as increases in the temperature and nanosilica concentration will both decrease the PV values. The effect of mud weight, in contrast, results in higher PV values. This result is due to the higher solid content in a heavier mud, which leads to a decrease in the distance among bentonite particles and an increase in the frictional force [91].

3.2.11. YP of 12 ppg WBM samples with and without nanosilica

Fig. 43 shows the YPs obtained for the 12 ppg WBM samples with and without nanosilica before and after hot rolling. The recommended range for the YP of a WBM is less than or equal to 50 lb/100 sq ft for before hot rolling and low temperature hot rolling conditions and between 10 and 25 lb/100 sq ft for high temperature hot rolling conditions.

As displayed in Fig. 43, only four samples are within the recommended range, and they are all samples that have been aged at high temperatures: the 1.0 ppb and 1.5 ppb nanosilica WBMs hot rolled at 250 °F and 300 °F. After 250 °F and 300 °F hot rolling, the YPs obtained for the 1.0 and 1.5 ppb nanosilica WBM are 18 and 22 lb/100 sq ft, respectively. The 1.0 ppb nanosilica sample shows the greatest reduction in the YP relative to its basic mud at all conditions.

However, the samples before aging and after aging at low temperature exhibit rather high YPs, which are very undesirable as a high YP leads to flocculation, decreases in the ROP and escalation of the surge and swap pressure. As mentioned earlier, the YP is a parameter

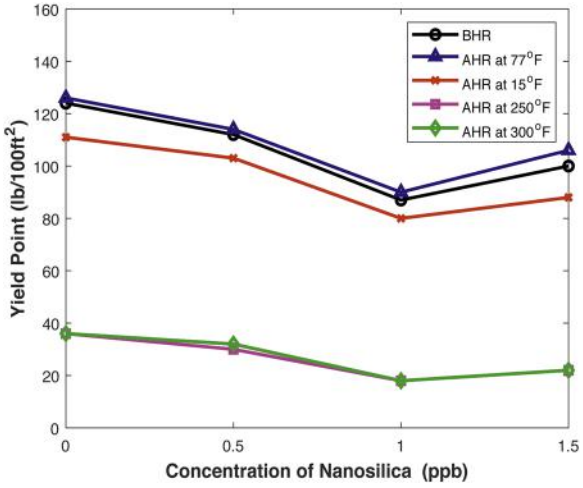

Fig. 43. YP of 12 ppg WBM samples with and without nanosilica.

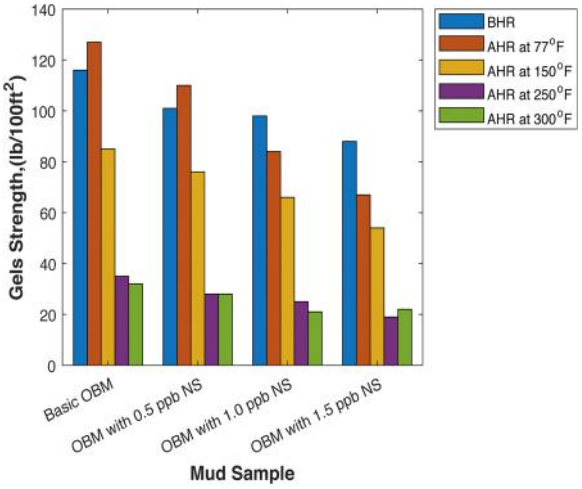

Fig. 45. GS at 10 m of 12 ppg WBM samples with and without nanosilica.

that is closely related to the PV, and the YPs are higher for the 12 ppg WBMs because heavier muds have a higher solid content and a higher solid content will results in a higher PV and hence a higher YP [15].

3.2.12. GS at 10 s of 12 ppg WBM samples with and without nanosilica

Fig. 44 demonstrates the 10 s GSs of the 12 ppg WBM samples with and without nanosilica before and after aging. The ideal 10 s GS that a WBM should have is less than or equal to 15 lb/100 sq ft.

As shown in Fig. 44, 6 samples are within the ideal specifications suggested. These samples are all nanosilica-enhanced WBM samples aged at high temperature. For the samples that have undergone aging at 250 °F, the 10 s GSs displayed by the 0.5 ppb, 1.0 ppb and 1.5 ppb nanosilica samples are 15, 14 and 14 lb/100 sq ft, respectively. As for those aged at 300 °F, the 0.5 ppb, 1.0 ppb and 1.5 ppb nanosilica samples have 10 s GSs of 12 lb/100 sq ft, 10 lb/100 sq ft and 10 lb/100 sq ft, respectively.

The concentration and temperature effects on the 12 ppg 10 s GS are similar to those on the 9 ppg 10 s GS. As for the impact of mud weight, since the GS of a drilling mud is closely associated with both its PV and YP, a higher PV mud sample will have a higher GS due to the higher solid content.

3.2.13. GS at 10 m of 12 ppg WBM samples with and without nanosilica

Fig. 45 illustrates the 10 m GSs of 12 ppg WBM samples with and without nanosilica both before aging and after aging. The recommended specification for the 10 m GS is that it be less than or equal to 35 lb/100 sq ft for both high temperature and low temperature conditions.

As portrayed in Fig. 45, all the samples aged at high temperature successfully satisfy the recommended specification. For these samples, an increase of the nanosilica concentration increases the reduction of the 10 m GS of a mud sample relative to its basic mud. The 10 m GSs exhibited by the basic mud and 0.5 ppb, 1.0 ppb and 1.5 ppb nanosilica samples aged at 250 °F are 35 lb/100 sq ft, 28 lb/100 sq ft, 25 lb/100 sq ft and 19 lb/100 sq ft. Meanwhile, the basic mud and 0.5 ppb, 1.0 ppb and 1.5 ppb nanosilica samples that have undergone aging at 300 °F have 10 m GSs of 32 lb/100 sq ft, 28 lb/100 sq ft, 21 lb/100 sq ft and 22 lb/100 sq ft.

The effects of nanosilica concentration, temperature and mud weight are similar to those for the 10 s GS.

A comparison is performed between the 10 s and 10 m GSs of each sample in order to examine the formation of a progressive gel, which is relatively important in enabling the instant resumption of mud circulation as well as suspension of cuttings. The results are plotted in Fig. 46.

Fortunately, all samples can form progressive gels, as there are appreciable ranges between the 10 s and 10 m GSs of each sample.

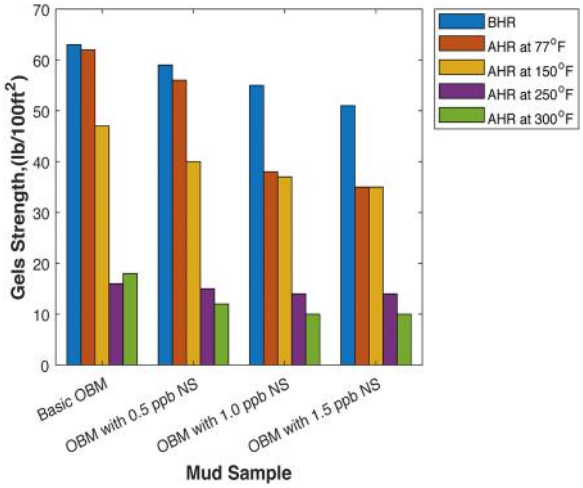

Fig. 44. GS at 10 s of 12 ppg WBM samples with and without nanosilica.

3.2.14. API filtration of 12 ppg WBM samples with and without nanosilica

Fig. 47 portrays the API filtration results for the 12 ppg WBM samples with and without nanosilica before and after aging. The suggested range of API fluid loss is less than or equal to 15 cc for 30 min of filtration, and this range applies to both low and high temperature conditions.

As shown in Fig. 47, the pattern observed in the API filtration of 12 ppg WBM is similar to that of 9 ppg WBM, in which only the before aging samples show a decrease in the fluid loss volume with increasing nanosilica concentration, while the other samples display a trend in which the fluid loss volume increases proportionally with the nanosilica concentration. Despite this result, only two samples are outside the suggested range: the 1.5 ppb nanosilica samples aged at 250 °F and 300 °F, showing fluid loss volumes of 16.6 cc and 18.4 cc, respectively.

The effect of temperature on the API fluid loss of 12 ppg WBM is similar to that of the 9 ppg WBM. However, the filtration of 12 ppg WBM is improved based on a comparison with 9 ppg WBM; the impact of the high mud weight reduces the fluid loss volume. This reduction can be explained by the higher solid content that occurs with the increase of the mud weight; as mentioned earlier, a higher solid content decreases the distance between bentonite particles, which enables packing to occur, thus forming a better mud cake that in turn reduces fluid loss.

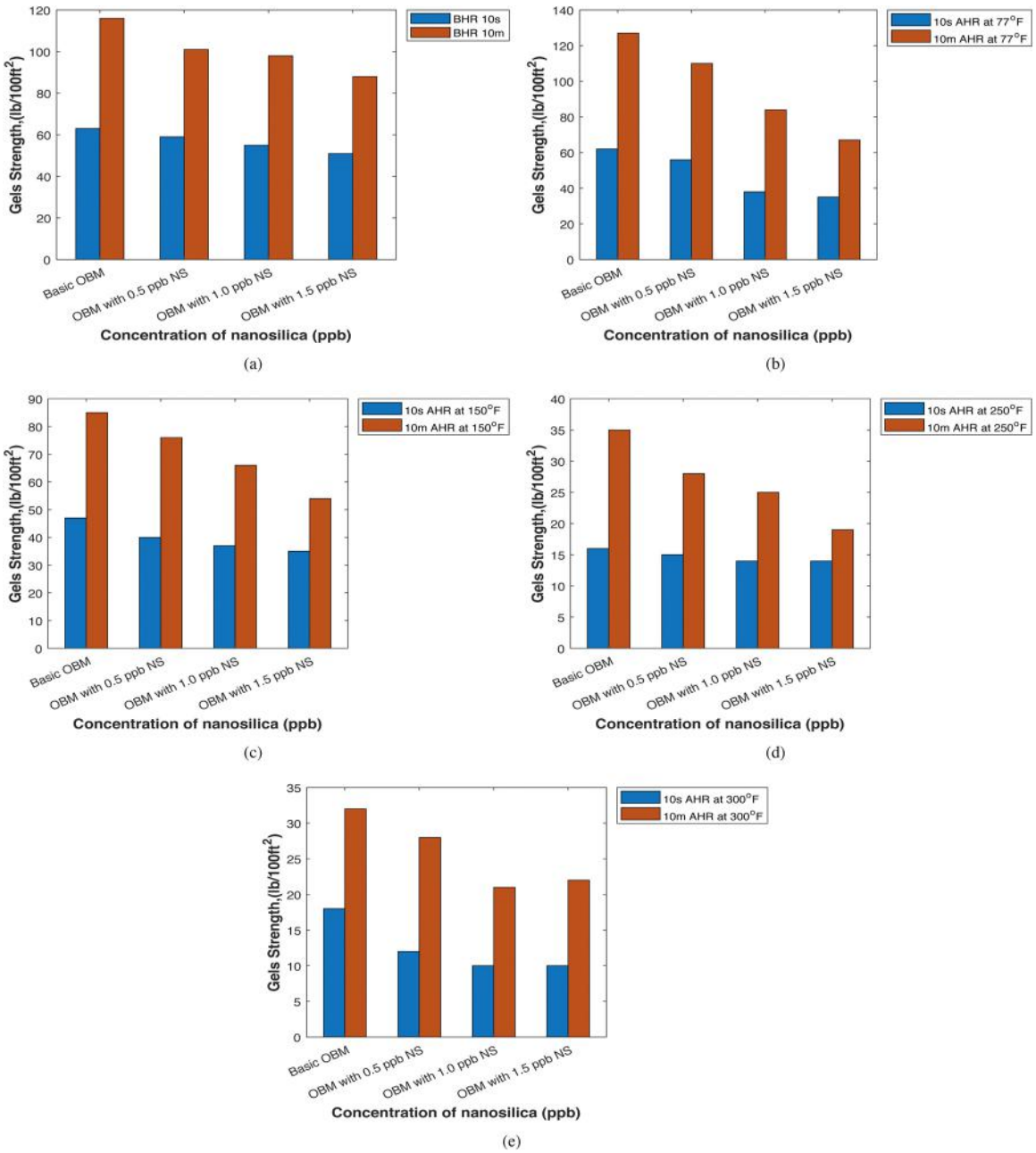

Fig. 46. Comparison of 10 s and 10 m GSs of 12 ppg WBM samples with different aging temperatures: (a) before aging, (b) after aging at 77 °F, (c) after aging at 150 °F, (d) after aging at 250 °F and (e) after aging at 300 °F.

3.2.15. API mud cake thickness of 12 ppg WBM samples with and without nanosilica

Fig. 48 displays the API mud cake thicknesses obtained for the 12 ppg mud samples subjected to the API filtration test. The ideal range of the API mud cake thickness is less than or equal to 3/32 inches.

According to Fig. 48, only two samples are outside the ideal specification range, similar to the API filtration loss. These samples are the 1.5 ppb nanosilica WBM samples aged at 250 °F and 300 °F, each having thicknesses of 4/32 inches. Since the API filtration loss and API mud cake thickness are closely related, they are proportional to each other.

The effects of temperature, nanosilica concentration and mud weight are similar to those mentioned in the API filtration section.

3.2.16. HPHT filtration of 12 ppg WBM samples with and without nanosilica

Fig. 49 illustrates the HPHT filtration of the 12 ppg WBM samples aged at a high temperature ranging from 250 °F to 300 °F. The range of HPHT filtrate loss suggested by Scomi [97] Oil Tools is less than or equal to 25 cc for 30 min of filtration.

As shown in Fig. 49, all the mud samples are within the recommended range, showing HPHT filtration losses of less than 25 cc for 30 min. An increase in the nanosilica concentration increases the fluid loss, similar to the pattern observed for the HPHT filtration of the 9 ppg WBM samples.

Additionally, the effect of mud weight positively impacts the losses, as heavier mud has a lower filtration loss. This result occurs for the same reason mentioned for API filtration.

3.2.17. HPHT mud cake thickness of 12 ppg WBM samples with and without nanosilica

Fig. 50 displays the HPHT mud cake thicknesses obtained for the 12 ppg WBM samples subjected to the HPHT filtration test. The range

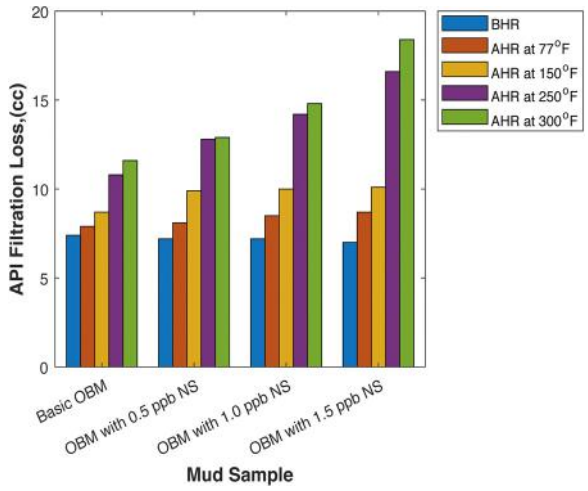

Fig. 47. API filtration of 12 ppg WBM with and without nanosilica.

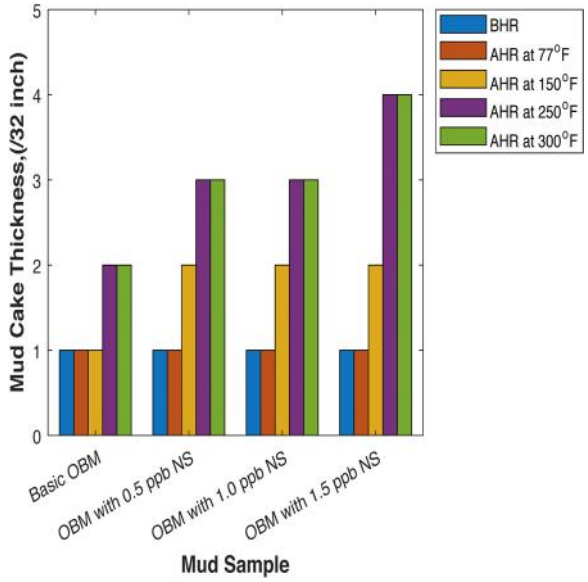

Fig. 48. API mud cake thickness of 12 ppg WBM with and without nanosilica.

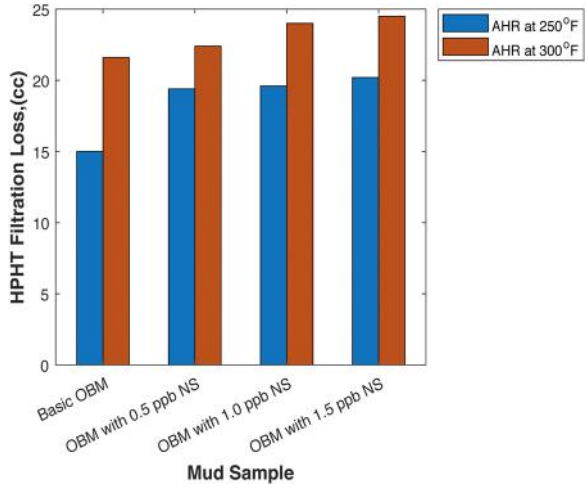

Fig. 49. HPHT filtration of 12 ppg WBM with and without nanosilica.

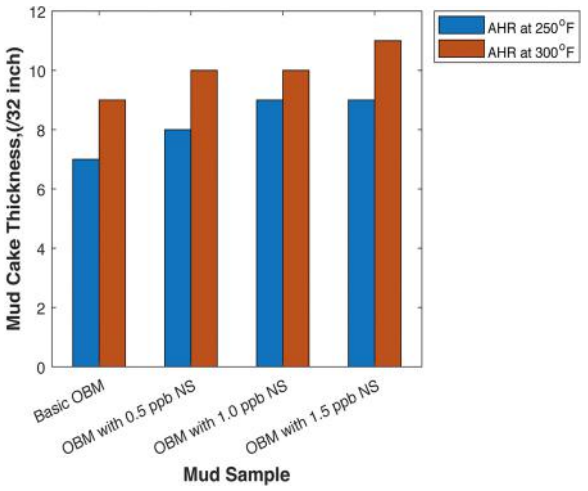

Fig. 50. HPHT mud cake thickness of 12 ppg WBM with and without nanosilica.

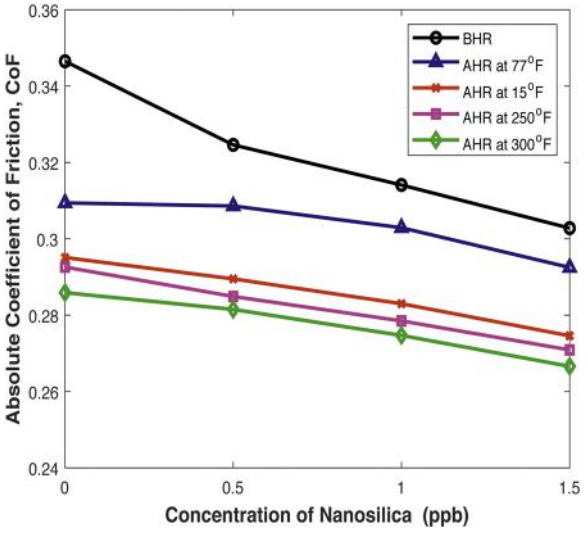

Fig. 51. CoF of 12 ppg WBM samples with and without nanosilica.

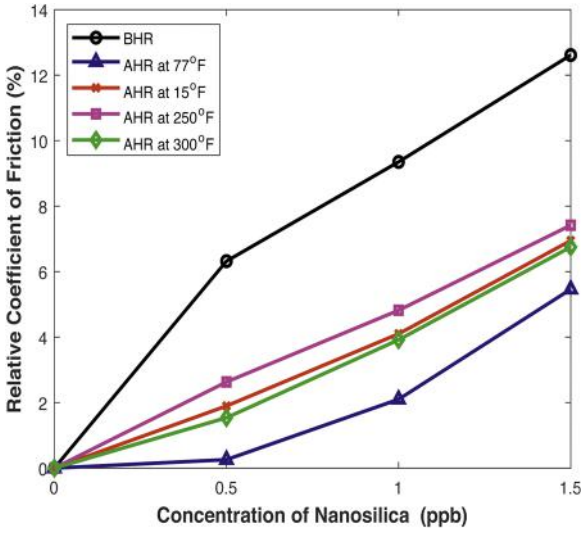

Fig. 52. Relative CoF reduction of 12 ppg WBM samples with and without nanosilica.

Table 14
Modelled equations for 9 ppg WBM basic mud.

Model	Equation	Parameters				Error (%)
		τ_o, τ_y	k	n	μ_p or, μ_d	
Newtonian [9]	Undefined					
Bingham [93]	$\tau = 0.0094 \cdot \gamma + 17.9038$	17.938			0.0094	
HerschelBulkley [94]	Undefined					
OstwaldPower Law [95]	$\tau = 17.0302 \cdot \gamma^{0.0261}$		17.0302	0.0261	34.66	

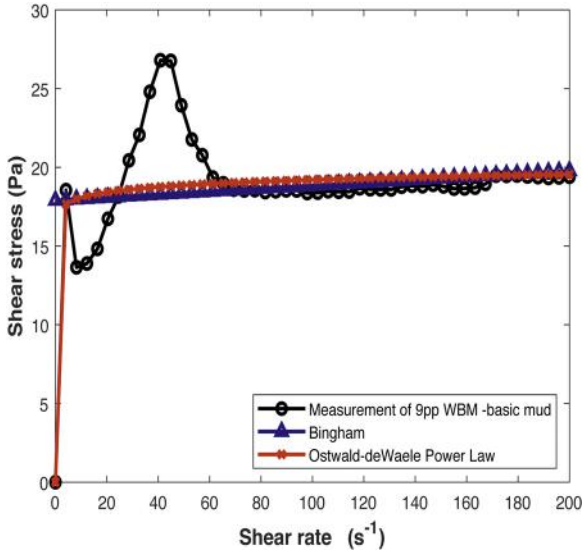

Fig. 53. Rheological modeling of 9 ppg WBM basic mud.

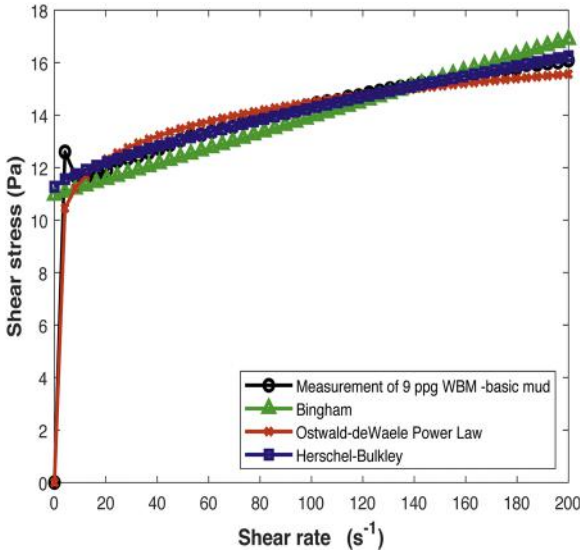

Fig. 54. Rheological modeling of 9 ppg WBM basic mud with 1.0 ppb nanosilica.

for this property recommended by Scomi [97] Oil Tools is less than or equal to 10/32 inches after 30 min of filtration.

As plotted in Fig. 50, only one sample is not within the ideal range: the 1.5 ppb nanosilica WBM sample that experiences the highest HPHT filtration loss, which has a mud cake thickness of 11/32 inches.

Since the HPHT mud cake thickness is proportional to the HPHT filtration loss, the impacts of temperature, nanosilica concentration and mud weight are the same as those for HPHT filtration.

3.2.18. Lubricity of 12 ppg WBM samples with and without nanosilica

Fig. 51 demonstrates the CoF values of the 12 ppg WBM samples with and without nanosilica both before and after aging, while Fig. 52 displays the reduction of the CoF of every nanosilica-enhanced sample relative to its basic mud at the respective condition.

Similar to the other samples, an increase in the nanosilica concentration in the 12 ppg WBM proportionally increases the reduction of the CoF, as the smallest CoF values are obtained with the usage of 1.5 ppb nanosilica. With the addition of 1.5 ppb nanosilica under the before aging and aging at 77 °F to 300 °F conditions, the CoF values obtained are 0.303, 0.293, 0.275, 0.271 and 0.267.

According to Fig. 51, the 1.5 ppb nanosilica muds before aging and after aging at 77 °F to 300 °F exhibit relative CoF reductions of 12.61%, 5.46%, 6.95%, 7.42% and 6.75%.

3.2.19. Rheological modeling of WBM samples with and without nanosilica

Rheological modeling is again conducted to investigate which rheological model best describes the selected water-based drilling fluid sample. The selected samples for this rheological modeling are the basic mud of each mud weight as well as the WBM samples that contain 1.0 ppb nanosilica because, overall, the 1.0 ppb nanosilica WBM samples have performed optimally in terms of almost all the rheological properties examined. Moreover, the type of rheological models investigated are the Newtonian [9], Bingham [93], Herschel-Bulkley [94] and Ostwald power law [95] models.

The results obtained from the modeling of the 9 ppg WBM basic mud sample are tabulated and plotted in Table 14 and Fig. 53, respectively.

Referring to Fig. 53, both the Bingham plastic and Ostwald models' trend lines are fairly close the 9 ppg basic mud trend line. However, the rheological model that best describes the mud sample is the Ostwald [95] model, as its deviation error is only 34.66%, which is less than the error observed for the Bingham plastic model.

The modeling results for the 9 ppg WBM sample containing 1.0 ppb

Table 15
Modelled equations for 9 ppg WBM with 1.0 ppb of nanosilica.

Model	Equation	Parameters				Error (%)
		τ_o,τ_y	k	n	μ_p or μ_d	
Newtonian [9]	Undefined					
Bingham [93]	$\tau = 0.0297 \cdot \gamma + 10.9452$	10.9452			0.0297	7.46
HerschelBulkley [94]	$\tau = 11.27 + 0.1041(\cdot \gamma^{0.7297})$	11.27	0.1041	0.7297		2.8
OstwaldPower Law [95]	$\tau = 9.0539 \cdot \gamma^{0.1022}$		9.0539	0.1022	6.5	

Table 16
Modelled equations for 12 ppg basic WBM.

Model	Equation	Parameters				Error (%)
		τ_o, τ_y	k	n	μ_p or μ_d	
Newtonian [9]	Undefined					
Bingham [93]	$\tau = -0.0241 \cdot \gamma + 49.9525$	49.9525			−0.0241	137.4
HerschelBulkley [94]	Undefined					
OstwaldPower Law [95]	$\tau = 62.9267 \cdot \gamma^{-0.0601}$		62.9267	−0.0601	91.1	

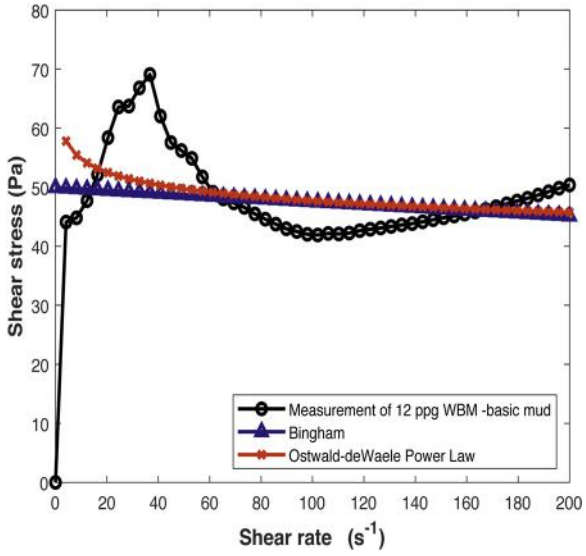

Fig. 55. Rheological modeling of 12 ppg basic WBM.

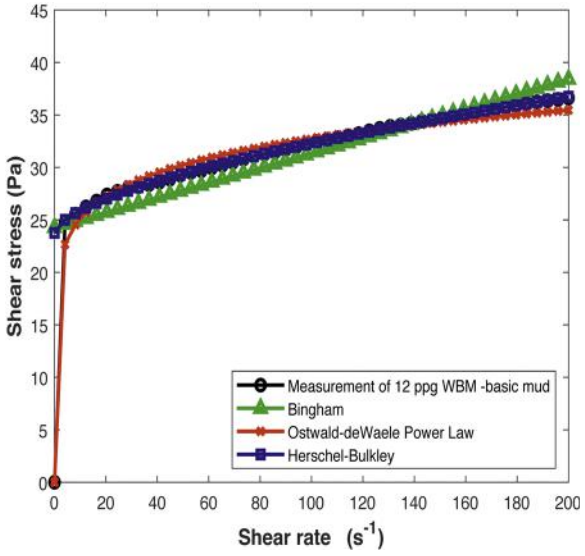

Fig. 56. Rheological modeling of 12 ppg WBM with 1.0 ppb nanosilica.

nanosilica are tabulated and plotted in Table 15 and Fig. 54, respectively.

As shown in Fig. 54, the trend line generated from the 9 ppg WBM containing 1.0 ppb nanosilica matches that of the Herschel-Bulkley [94] model even at the beginning of the figure. This result is confirmed by the deviation error in Table 4.9, showing that the difference between the Herschel-Bulkley [94] model and the WBM sample is only 2.8%, while the other models have larger deviations.

The modeling results obtained for the 12 ppg basic WBM are tabulated and plotted in Table 16 and Fig. 55, respectively.

According to Fig. 55, the trend line generated from the 12 ppg basic mud sample does not follow any rheological model investigated. Referring to the tabulated data, the deviation error percentages of this mud sample for both the Bingham [93] and Ostwald [95] models are very high, with values of 137.4% and 91.1%, respectively.

The final WBM sample submitted to rheological modeling is the 12 ppg WBM sample containing 1.0 ppb nanosilica. Its modeling data are tabulated and plotted in Table 17 and Fig. 56, respectively.

As shown in Fig. 56, the trend line of the 12 ppg WBM with 1.0 ppb nanosilica better matches that of the Herschel–Bulkley [94] model than the other lines. This result is supported by the deviation error percentage of only 1.6%, which is significant less than those of the other models. Hence, the most suitable model to describe the fluid properties of 12 ppg WBM with 1.0 ppb nanosilica is the Herschel–Bulkley [94] model.

4. Conclusions

The following conclusions are drawn from this study:

1. Nanosilica can be effectively dispersed without using an ultrasonicator by only altering the pH of the mud, which results in surface repulsion of nanosilica.
2. The usage of nanosilica can effectively improve most of the rheological properties of both WBM and OBM even though the API and HPHT fluid losses have yet to be successfully improved.
3. The results indicate that the optimum concentration of nanosilica showing the most promising rheological properties for OBM is 0.5 ppb.
4. From the results discussed, the optimum concentration of nanosilica that can optimally enhance the rheological properties of WBM is 1.0 ppb.
5. All the OBM and WBM samples containing nanosilica follow the Herschel–Bulkley [94] model, while only the basic WBM samples

Table 17
Modelled equations for 12 ppg WBM with 1.0 ppb of nanosilica.

Model	Equation	Parameters				Error (%)
		τ_o, τ_y	k	n	μ_p or μ_d	
Newtonian [9]	Undefined					
Bingham [93]	$\tau = 0.07061 \cdot \gamma + 24.283$	24.283		0.0706		0.0706
HerschelBulkley [94]	$\tau = 23.7651 \cdot \gamma + 0.5288 \cdot \gamma^{0.6038}$	23.7651	0.5288	0.6038		1.6
OstwaldPower Law [95]	$\tau = 19.2798 \cdot \gamma^{0.115}$		19.2798	0.115	10.8	

follow the Ostwald [95] power law.

Conflict of interest

The authors declare no conflicting interests.

Appendix A

Table 18

Table 18
Typical properties of Sarapar 147.

Component	Chemical composition (%m)
N-Paraffins	95 minimum
Iso-paraffins	< 5
Napthanics	< 0.1
Aromatics	< 0.01
Density	773 kg/m^3 at 15 °C
Sulphur	< 3 ppm
Boiling range	258–293 °C
Flash point	120 °C
Pour point	12 °C
Vk40	2.5 mm^2/s

Acknowledgements

The authors wish to express their sincere thanks to the Research Management Centre of University of Technologi Malaysia and the Malaysian Ministry of Higher Learning for providing the needed funds (Vote 4F575).

References

[1] S. Perween, N.K. Thakur, M. Beg, S. Sharma, A. Ranjan, Enhancing the properties of water based drilling fluid using bismuth ferrite nanoparticles, Colloids Surf. A Physicochem. Eng. Asp. 561 (2019) 165–177, https://doi.org/10.1016/j.colsurfa.2018.10.060.
[2] S.-Q. Hao, Development of portable drilling fluid and seepage simulation for deep saline aquifers, J. Pet. Sci. Eng. 175 (2019) 560–572, https://doi.org/10.1016/j.petrol.2018.12.070.
[3] N.F. Majid, A. Katende, I. Ismail, F. Sagala, N.M. Sharif, M.A.C. Yunus, A comprehensive investigation on the performance of durian rind as a lost circulation material in water based drilling mud, Petroleum (2019), https://doi.org/10.1016/j.petlm.2018.10.004.
[4] G. Jiang, S. Peng, X. Li, L. Yang, J.B.P. Soares, G. Li, Preparation of amphoteric starch-based flocculants by reactive extrusion for removing useless solids from water-based drilling fluids, Colloids Surf. A Physicochem. Eng. Asp. 561 (2019) 343–350, https://doi.org/10.1016/j.colsurfa.2018.08.077.
[5] S. Salehi, S.A. Madani, R. Kiran, Characterization of drilling fluids filtration through integrated laboratory experiments and CFD modeling, J. Nat. Gas Sci. Eng. 29 (2016) 462–468, https://doi.org/10.1016/j.jngse.2016.01.017.
[6] W.J. Yeu, A. Katende, F. Sagala, I. Ismail, Improving hole cleaning using low density polyethylene beads at different mud circulation rates in different hole angles, J. Nat. Gas Sci. Eng. 61 (2019) 333–343, https://doi.org/10.1016/j.jngse.2018.11.012.
[7] H. Hakim, A. Katende, F. Sagala, I. Ismail, H. Nsamba, Performance of polyethylene and polypropylene beads towards drill cuttings transportation in horizontal wellbore, J. Pet. Sci. Eng. 165 (2018) 962–969, https://doi.org/10.1016/j.petrol.2018.01.075.
[8] Y. Feng, K.E. Gray, Review of fundamental studies on lost circulation and wellbore strengthening, J. Pet. Sci. Eng. 152 (2017) 511–522, https://doi.org/10.1016/j.petrol.2017.01.052.
[9] P. Skalle, Drilling Fluid Engineering, Ventus Publishing Company, 2010.
[10] F. Growcock, T. Harvey, Drilling Fluids Processing Handbook, Elsevier, 2005.
[11] S. Talabani, G. Chukwu, D. Hatzignatiou, Drilling Successfully Through Deforming Shale Formations: Case Histories, Society of Petroleum Engineers, Low Permeability Reservoirs Symposium, 26–28 April, Denver, Colorado, 1993, pp. 1–7, , https://doi.org/10.2118/25867-MS.
[12] A.R. Ismail, A. Aftab, Z.H. Ibupoto, N. Zolkifil, The novel approach for the enhancement of rheological properties of water-based drilling fluids by using multi-walled carbon nanotube, nanosilica and glass beads, J. Pet. Sci. Eng. 139 (2016) 264–275, https://doi.org/10.1016/j.petrol.2016.01.036.
[13] H. Mao, Z. Qiu, Z. Shen, W. Huang, H. Zhong, W. Dai, Novel hydrophobic associated polymer based nano-silica composite with core-shell structure for intelligent drilling fluid under ultra-high temperature and ultra-high pressure, Prog. Nat. Sci. Mater. Int. 25 (1) (2015) 90–93, https://doi.org/10.1016/j.pnsc.2015.01.013.
[14] A.E. Bayat, P.J. Moghanloo, A. Piroozian, R. Rafati, Experimental investigation of rheological and filtration properties of water-based drilling fluids in presence of various nanoparticles, Colloids Surf. A Physicochem. Eng. Asp. 555 (2018) 256–263, https://doi.org/10.1016/j.colsurfa.2018.07.001.
[15] A.H. Salih, H. Bilgesu, Investigation of Rheological and Filtration Properties of Water-Based Drilling Fluids Using Various Anionic Nanoparticles, Society of Petroleum Engineers, SPE Western Regional Meeting, 23–27 April, Bakersfield, California, 2017, https://doi.org/10.2118/185638-MS.
[16] S. Alkhalaf, M. Alawami, V. Wagle, A. Al-Yami, Less Damaging Drilling Fluids: Development and Lab Testing, International Petroleum Technology Conference, International Petroleum Technology Conference, 26–28 March, Beijing, China, 2019, https://doi.org/10.2523/19205-MS.
[17] M. Al-Yasiri, A. Awad, S. Pervaiz, D. Wen, Influence of silica nanoparticles on the functionality of water-based drilling fluids, J. Pet. Sci. Eng. (2019), https://doi.org/10.1016/j.petrol.2019.04.081.
[18] N. Jafariesfad, M. Khalifeh, P. Skalle, M.R. Geiker, Nanorubber-modified cement system for oil and gas well cementing application, J. Nat. Gas Sci. Eng. 47 (2017) 91–100, https://doi.org/10.1016/j.jngse.2017.10.002.
[19] Z.A. Dijvejin, A. Ghaffarkhah, S. Sadeghnejad, M.V. Sefti, Effect of silica nanoparticle size on the mechanical strength and wellbore plugging performance of SPAM/chromium (III) acetate nanocomposite gels, Polym. J. (2019), https://doi.org/10.1038/s41428-019-0178-3.
[20] L. Hendraningrat, S. Li, O. Torsaeter, A coreflood investigation of nanofluid enhanced oil recovery, J. Pet. Sci. Eng. 111 (2013) 128–138, https://doi.org/10.1016/j.petrol.2013.07.003.
[21] R.C. Aadland, T.D. Jakobsen, E.B. Heggset, H. Long-Sanouiller, S. Simon, K.G. Paso, K. Syverud, O. Torsaeter, High-temperature core flood investigation of nanocellulose as a green additive for enhanced oil recovery, Nanomaterials 9 (5) (2019), https://doi.org/10.3390/nano9050665.
[22] S.I. Reilly, Z. Vryzas, V.C. Kelessidis, D.I. Gerogiorgis, First-principles rheological modelling and parameter estimation for nanoparticle-based smart drilling fluids, Comput. Aided Chem. Eng. 38 (2016) 1039–1044, https://doi.org/10.1016/B978-0-444-63428-3.50178-8.
[23] L. Whatley, R. Barati, Z. Kessler, J.-S. Tsau, Water-Based Drill-In Fluid Optimization Using Polyelectrolyte Complex Nanoparticles as a Fluid Loss Additive, Society of Petroleum Engineers, SPE International Conference on Oilfield Chemistry, 8–9 April, Galveston, TX, USA, 2019, https://doi.org/10.2118/193544-MS.
[24] J. Aramendiz, A. Imqam, Water-based drilling fluid formulation using silica and graphene nanoparticles for unconventional shale applications, J. Pet. Sci. Eng. (2019), https://doi.org/10.1016/j.petrol.2019.04.085.
[25] R. Rafati, S.R. Smith, A.S. Haddad, R. Novara, H. Hamidi, Effect of nanoparticles on the modifications of drilling fluids properties: a review of recent advances, J. Pet. Sci. Eng. 161 (2018) 61–76, https://doi.org/10.1016/j.petrol.2017.11.067.
[26] A.O. Gbadamosi, R. Junin, Y. Abdalla, A. Agi, J.O. Oseh, Experimental investigation of the effects of silica nanoparticle on hole cleaning efficiency of water-based drilling mud, J. Pet. Sci. Eng. 172 (2019) 264–275, https://doi.org/10.1016/j.petrol.2018.09.097.
[27] A. Parizad, K. Shahbazi, A.A. Tanha, Enhancement of polymeric water-based drilling fluid properties using nanoparticles, J. Pet. Sci. Eng. 170 (2018) 813–828, https://doi.org/10.1016/j.petrol.2018.06.081.
[28] M. Riley, E. Stamatakis, K. Price, S. Young, G.D. Stefano, Novel Water Based Mud for Shale Gas Part II: Mud Formulation and Performance, Society of Petroleum Engineers, SPE/EAGE European Unconventional Resources Conference and Exhibition, 20–22 March, Vienna, Austria, 2004, https://doi.org/10.2118/152945-MS.

[29] Z. Vryzas, L. Nalbandian, V.T. Zaspalis, V.C. Kelessidis, How different nanoparticles affect the rheological properties of aqueous Wyoming sodium bentonite suspensions, J. Pet. Sci. Eng. 173 (2019) 941–954, https://doi.org/10.1016/j.petrol.2018.10.099.
[30] A.I. El-Diasty, A.M.S. Ragab, Applications of Nanotechnology in the Oil and Gas Industry: Latest Trends Worldwide and Future Challenges in Egypt, Society of Petroleum Engineers, North Africa Technical Conference and Exhibition, 15–17 April, Cairo, Egypt, 2013, https://doi.org/10.2118/164716-MS.
[31] M. Amanullah, M.K. AlArfaj, Z.A. Al-abdullatif, Preliminary Test Results of Nano-based Drilling Fluids for Oil and Gas Field Application, Society of Petroleum Engineers, SPE/IADC Drilling Conference and Exhibition, 1–3 March, Amsterdam, The Netherlands, 2013, https://doi.org/10.2118/139534-MS.
[32] M. Amanullah, A.M. Al-Tahini, Nano-Technology – Its Significance in Smart Fluid Development for Oil and Gas Field Application, Society of Petroleum Engineers, SPE Saudi Arabia Section Technical Symposium, 9–11 May, Al-Khobar, Saudi Arabia, 2009, https://doi.org/10.2118/126102-MS.
[33] J.K.M. William, S. Ponmani, R. Samuel, R. Nagarajan, J.S. Sangwaia, Effect of CuO and ZnO nanofluids in xanthan gum on thermal, electrical and high pressure rheology of water-based drilling fluids, J. Pet. Sci. Eng. 117 (2014) 15–27, https://doi.org/10.1016/j.petrol.2014.03.005.
[34] M. Sadeghalvaad, S. Sabbaghi, The effect of the TiO2/polyacrylamide nanocomposite on water-based drilling fluid properties, Powder Technol. 272 (2015) 113–119, https://doi.org/10.1016/j.powtec.2014.11.032.
[35] M.M. Sharma, R. Zhang, M.E. Chenevert, L. Ji, Q. Guo, J. Friedheim, A New Family of Nanoparticle Based Drilling Fluids, Society of Petroleum Engineers, SPE Annual Technical Conference and Exhibition, 8–10 October, San Antonio, TX, USA, 2012, https://doi.org/10.2118/160045-MS.
[36] K. Song, Q. Wu, M.-C. Li, A.K. Wojtanowicz, L. Dong, X. Zhang, S. Ren, T. Lei, Performance of low solid bentonite drilling fluids modified by cellulose nanoparticles, J. Nat. Gas Sci. Eng. 34 (2016) 1403–1411, https://doi.org/10.1016/j.jngse.2016.08.036.
[37] T.T. Yi, I. Ismail, A. Katende, F. Sagala, J. Mugisa, Experimental investigation of cuttings lifting efficiency using low and high density polyethylene beads in different hole angles, J. Mater. Sci. Appl. 3 (5) (2017) 71–78 http://article.aascit.org/file/pdf/8910898.pdf.
[38] A. Kazemi-Beydokhti, S.H. Hajiabadi, Rheological investigation of smart polymer/carbon nanotube complex on properties of water-based drilling fluids, Colloids Surf. A Physicochem. Eng. Asp. 556 (2018) 23–29, https://doi.org/10.1016/j.colsurfa.2018.07.058.
[39] C. PeterEzeakacha, S. Salehi, Experimental and statistical investigation of drilling fluid loss in porous media: Part 2 (Fractures), J. Nat. Gas Sci. Eng. 65 (2019) 257–266, https://doi.org/10.1016/j.jngse.2019.03.007.
[40] G. Cheraghian, Q. Wu, M. Mostofi, M.-C. Li, M. Afrand, J.S. Sangwaif, Effect of a novel clay/silica nanocomposite on water-based drilling fluids: improvements in rheological and filtration properties, Colloids Surf. A Physicochem. Eng. Asp. 555 (2018) 339–350, https://doi.org/10.1016/j.colsurfa.2018.06.072.
[41] J.T. Srivatsa, M.B. Ziaja, An Experimental Investigation on Use of Nanoparticles as Fluid Loss Additives in a Surfactant – Polymer Based Drilling Fluids, International Petroleum Technology Conference, International Petroleum Technology Conference, 15–17 November, Bangkok, Thailand, 2004, https://doi.org/10.2523/IPTC-14952-MS.
[42] M. Zakaria, M.M. Husein, G. Harland, Novel Nanoparticle-Based Drilling Fluid with Improved Characteristics, Society of Petroleum Engineers, SPE International Oilfield Nanotechnology Conference and Exhibition, 12–14 June, Noordwijk, The Netherlands, 2012, https://doi.org/10.2118/156992-MS.
[43] M.M. Barry, Y. Jung, J.-K. Lee, T.X. Phuoc, M.K. Chyu, Fluid filtration and rheological properties of nanoparticle additive and intercalated clay hybrid bentonite drilling fluids, J. Pet. Sci. Eng. 127 (2015) 338–346, https://doi.org/10.1016/j.petrol.2015.01.012.
[44] E.U. Akpan, G.C. Enyi, G. Nasr, A.A. Yahaya, A.A. Ahmadu, B. Saidu, Water-based drilling fluids for high-temperature applications and water-sensitive and dispersible shale formations, J. Pet. Sci. Eng. 175 (2019) 1028–1038, https://doi.org/10.1016/j.petrol.2019.01.002.
[45] S. Riisoen, F. Iversen, R. Brasileiro, A. Saasen, M. Khalifeh, Drilling Fluid Power-Law Viscosity Model – Impact of Model Parameters on Frictional Pressure Loss Uncertainty, Society of Petroleum Engineers, SPE Norway One Day Seminar, 14 May, Bergen, Norway, 2019, https://doi.org/10.2118/195623-MS.
[46] A. Aftab, A.R. Ismail, Z.H. Ibupoto, H. Akeiber, M.G.K. Malghani, Nanoparticles based drilling muds a solution to drill elevated temperature wells: a review, Renew. Sustain. Energy Rev. 76 (2017) 1301–1313, https://doi.org/10.1016/j.rser.2017.03.050.
[47] A. Aftab, A.R. Ismail, Z.H. Ibupoto, Enhancing the rheological properties and shale inhibition behavior of water-based mud using nanosilica, multi-walled carbon nanotube, and graphene nanoplatelet, Egypt. J. Pet. 26 (2017) 291–299, https://doi.org/10.1016/j.ejpe.2016.05.004.
[48] V.M. Oltedal, B. Werner, B. Lund, A. Saasen, J.D. Ytrehus, Rheological properties of oil based drilling fluids and base oils, Am. Soc. Mech. Eng. (2015) 1–8, https://doi.org/10.1115/OMAE2015-41911.
[49] P.J. Boul, B.R. Reddy, M. Hillfiger, T.P. O'Connell, C. Thaemlitz, Functionalized Nanosilicas as Shale Inhibitors in Water-Based Drilling Fluids, Offshore Technology Conference, Offshore Technology Conference, 2–5 May, Houston, TX, USA, 2016, https://doi.org/10.4043/26902-MS.
[50] API, Recommended Practice for Field Testing Water-based Drilling Fluids, (2009) (Online; accessed January-2019), http://ballots.api.org/ecs/sc13/API_RP13B-1_5Ed_TestingWBDF_4316.pdf.
[51] A.L. Barroso, C.P. Marcelino, A.B. Leal, D.M. Odum, C. Lucena, M. Masculo, F. Castro, New Generation Nano Technology Drilling Fluids Application Associated to Geomechanic Best Practices: Field Trial Record in Bahia – Brazil, Offshore Technology Conference, Offshore Technology Conference, 2–5 May, Houston, TX, USA, 2016, https://doi.org/10.4043/28731-MS.
[52] A. Addagalla, I. Maley, L. Moroni, M. Khafagy, Nano-Technology Based Bridging System Helps Drilling Success in Highly Depleted Mature Fields, Society of Petroleum Engineers, Abu Dhabi International Petroleum Exhibition and Conference, 12–15 November, Abu Dhabi, UAE, 2018, https://doi.org/10.2118/193153-MS.
[53] P.M. Mcelfresh, M. Wood, D. Ector, Stabilizing Nano Particle Dispersions in High Salinity, High Temperature Downhole Environments, Society of Petroleum Engineers, SPE International Oilfield Nanotechnology Conference and Exhibition, 12–14 June, Noordwijk, The Netherlands, 2012, https://doi.org/10.2118/154758-MS.
[54] S. Ghanbari, E. Kazemzadeh, M. Soleymani, A. Naderifar, A facile method for synthesis and dispersion of silica nanoparticles in water-based drilling fluid, J. Pet. Sci. Eng. 294 (2016) 381–388, https://doi.org/10.1007/s00396-015-3794-2.
[55] L. Ma, Y. He, P. Luo, L. Zhang, Y. Yu, Automatic dispersion, long-term stability of multi-walled carbon nanotubes in high concentration electrolytes, J. Nanopart. Res. 20 (45) (2018) 1–12, https://doi.org/10.1007/s11051-018-4148-z.
[56] W. Li, X. Zhao, Y. Ji, H. Peng, B. Chen, L. Liu, X. Han, Investigation of biodiesel-based drilling fluid, Part 1: Biodiesel evaluation, invert-emulsion properties, and development of a novel emulsifier package, society of petroleum engineers, SPE J. (2016), https://doi.org/10.2118/180918-PA.
[57] W. Li, X. Zhao, Y. Ji, H. Peng, B. Chen, L. Liu, X. Han, Investigation of biodiesel-based drilling fluid, Part 2: Formulation design, rheological study, and laboratory evaluation, society of petroleum engineers, SPE J. (2016), https://doi.org/10.2118/180926-PA.
[58] S.A. Wissing, O. Kayser, R.H. Muller, Solid lipid nanoparticles for parenteral drug delivery, Adv. Drug Deliv. Rev. 56 (9) (2004) 1257–1272, https://doi.org/10.1016/j.addr.2003.12.002.
[59] K. Ravichandran, R. Palaniraj, N.M.M.T.S. abd Ahmed, M.M. Gabr, A.R. Ahmed, D. Knorr, I. Smetanska, Effects of different encapsulation agents and drying process on stability of betalains extract, J. Food Sci. Technol. 51 (9) (2014) 1257–1272, https://doi.org/10.1007/s13197-012-0728-6.
[60] S. Honary, F. Zahir, Effect of zeta potential on the properties of nano-drug delivery systems – a review (part 1), Trop. J. Pharm. Res. 12 (2) (2013), https://doi.org/10.4314/tjpr.v12i2.19.
[61] N.V. Boyou, I. Ismail, W.R.W. Sulaiman, A.S. Haddad, N. Husein, H.T. Hui, K. Nadaraja, Experimental investigation of hole cleaning in directional drilling by using nano-enhanced water-based drilling fluids, J. Pet. Sci. Eng. 176 (2019) 220–231, https://doi.org/10.1016/j.petrol.2019.01.063.
[62] F.B. Growcock, C.F. Ellis, D.D. Schmidt, J.J. Azar, Electrical Stability, Emulsion Stability, and Wettability of Invert Oil-Based Muds, Society of Petroleum Engineers, SPE Drilling and Completion, 1994, https://doi.org/10.2118/20435-PA.
[63] S.G. Brush, Kinetic Theory: Irreversible Processes, Pergamon, 1966.
[64] A. Parizad, K. Shahbazi, A.A. Tanha, SiO2 nanoparticle and KCl salt effects on filtration and thixotropical behavior of polymeric water based drilling fluid: with zeta potential and size analysis, Results Phys. 9 (2018) 1656–1665, https://doi.org/10.1016/j.rinp.2018.04.037.
[65] R. Paramasivam, A.R. Ismail, Nanomaterial additive in oil based mud for high temperature condition, Young Petro (2016) 39–52 https://issuu.com/youngpetroart/docs/24.04-youngpetro-spring17-internet-.
[66] B. Werner, V. Myrseth, A. Saasen, Viscoelastic properties of drilling fluids and their influence on cuttings transport, J. Pet. Sci. Eng. 156 (2017) 845–851, https://doi.org/10.1016/j.petrol.2017.06.063.
[67] E.I. Epelle, D.I. Gerogiorgis*, A CFD investigation of the effect of particle sphericity on wellbore cleaning efficiency during oil and gas drilling, Comput. Aided Chem. Eng. 43 (2018) 127–132, https://doi.org/10.1016/B978-0-444-64235-6.50024-3.
[68] N.S.M. Heshamudin, A. Katende, H.A. Rashid, I. Ismail, F. Sagala, A. Samsuri, Experimental investigation of the effect of drill pipe rotation on improving hole cleaning using water-based mud enriched with polypropylene beads in vertical and horizontal wellbores, J. Pet. Sci. Eng. (2019).
[69] W. Li, X. Zhao, Y. Li, Y. Ji, H. Peng, L. Liu, Q. Yang, Laboratory investigations on the effects of surfactants on rate of penetration in rotary diamond drilling, J. Pet. Sci. Eng. 134 (2015) 114–122, https://doi.org/10.1016/j.petrol.2015.07.027.
[70] D. Kania, R. Yunus, R. Omar, S.A. Rashid, B.M. Jan, A review of biolubricants in drilling fluids: recent research, performance, and applications, J. Pet. Sci. Eng. 135 (2015) 177–184, https://doi.org/10.1016/j.petrol.2015.09.021.
[71] R.O. Afolabi, O.D. Orodu, V.E. Efeovbokhan, O.J. Rotimi, Z. Zhang, Optimizing the rheological properties of silica nano-modified bentonite mud using overlaid contour plot and estimation of maximum or upper shear stress limit, Cogent Eng. 4 (1) (2017) 1–18, https://doi.org/10.1080/23311916.2017.1287248.
[72] C. Vipulanandan, A. Mohammed, R.G. Samuel, Fluid Loss Control in Smart Bentonite Drilling Mud Modified with Nanoclay and Quantified with Vipulanandan Fluid Loss Model, Offshore Technology Conference, Offshore Technology Conference, 30 April–3 May, Houston, TX, USA, 2018, https://doi.org/10.4043/28947-MS.
[73] R.O. Afolabi, O.D. Orodu, I. Seteyeobot, Predictive modelling of the impact of silica nanoparticles on fluid loss of water based drilling mud, Appl. Clay Sci. 151 (2018) 37–45, https://doi.org/10.1016/j.clay.2017.09.040.
[74] C. Vipulanandan, A.R. Maddi, A.S. Ganpatye, Smart Spacer Fluid Modified with Iron Oxide Nanoparticles for In-Situ Property Enhancement was developed for Cleaning Oil Based Drilling Fluids and Characterized Using the Vipulanandan Rheological Model, Offshore Technology Conference, 30 April–3 May, Houston, TX, USA, 2018, pp. 1–20, , https://doi.org/10.4043/28886-MS.

[75] M.I. Abduo, A.S. Dahab, H. Abuseda, A.M. AbdulAziz, M.S. Elhossieny, Comparative study of using water-based mud containing multiwall carbon nanotubes versus oil-based mud in HPHT fields, Egypt. J. Pet. 25 (4) (2016) 459–464, https://doi.org/10.1016/j.ejpe.2015.10.008.
[76] A.A. Sulaimon, B.J. Adeyemi, M. Rahimi, Performance enhancement of selected vegetable oil as base fluid for drilling HPHT formation, J. Pet. Sci. Eng. 152 (2017) 49–59, https://doi.org/10.1016/j.petrol.2017.02.006.
[77] E. Nourafkan, M.A. Haruna, J. Gardy, D. Wen, Improved rheological properties and stability of multiwalled carbon nanotubes/polymer in harsh environment, J. Appl. Polym. Sci. 136 (11) (2019) 585–593, https://doi.org/10.1002/app.47205.
[78] A.R. Ismail, A. Aftab, Z.H. Ibupoto, N. Zolkifile, The novel approach for the enhancement of rheological properties of water-based drilling fluids by using multi-walled carbon nanotube, nanosilica and glass beads, J. Pet. Sci. Eng. 139 (2016) 264–275, https://doi.org/10.1016/j.petrol.2016.01.036.
[79] K. Anoop, R. Sadr, R. Yrac, M. Amani, Rheology of a colloidal suspension of carbon nanotube particles in a water-based drilling fluid, Powder Technol. 342 (2019) 585–593, https://doi.org/10.1016/j.powtec.2018.10.016.
[80] M. Amani, M. Al-Jubouri, A. Shadravan, Rheology of a colloidal suspension of carbon nanotube particles in a water-based drilling fluid, Adv. Pet. Explor. Dev. (2012) DOI: 1925543820120402.987/0.
[81] A. Aftab, A.R. Ismail, Z.H. Ibupoto, H. Akeiber, M.G.K. Malghani, Nanoparticles based drilling muds a solution to drill elevated temperature wells: a review, Renew. Sustain. Energy Rev. 76 (2017) 1301–1313, https://doi.org/10.1016/j.rser.2017.03.050.
[82] S.R. Smith, R. Rafati, A.S. Haddad, A. Cooper, H. Hamidi, Application of aluminium oxide nanoparticles to enhance rheological and filtration properties of water based muds at HPHT conditions, Colloids Surf. A Physicochem. Eng. Asp. 537 (2018) 361–371, https://doi.org/10.1016/j.colsurfa.2017.10.050.
[83] N. Wahid, M.A.M. Yusof, N.H. Hanafi, Optimum Nanosilica Concentration in Synthetic Based Mud (SBM) for High Temperature High Pressure Well, Society of Petroleum Engineers, SPE/IATMI Asia Pacific Oil & Gas Conference and Exhibition, 20–22 October, Nusa Dua, Bali, Indonesia, 2015, https://doi.org/10.2118/176036-MS.
[84] O.S. Guan, R. Gholami, A. Raza, M. Rabiei, N. Fakhari, V. Rasouli, O. Nabinezhad, A nano-particle based approach to improve filtration control of water based muds under high pressure high temperature conditions, Petroleum 5 (1) (2018), https://doi.org/10.1016/j.petlm.2018.10.006.
[85] M.S. Aston, P.J. Hearn, G. McGhee, Techniques for Solving Torque and Drag Problems in Today's Drilling Environment, Society of Petroleum Engineers, SPE Annual Technical Conference and Exhibition, 27–30 September, New Orleans, Louisiana, 1998, https://doi.org/10.2118/48939-MS.
[86] A. Wu, G. Hareland, Calculation of Friction Coefficient And Downhole Weight On Bit With Finite Element Analysis of Drillstring, American Rock Mechanics Association, 46th U.S. Rock Mechanics/Geomechanics Symposium, 24–27 June, Chicago, IL, 2012 https://www.onepetro.org/conference-paper/ARMA-2012-195.
[87] R. Samuel, Friction Factors: What are They for Torque, Drag, Vibration, Drill Ahead and Transient Surge/Swab Analysis, Society of Petroleum Engineers, IADC/SPE Drilling Conference and Exhibition, 2–4 February, New Orleans, LA, USA, 2010, https://doi.org/10.2118/128059-MS.
[88] M.C. Quigley, Advanced Technology for Laboratory Measurements of Drilling Fluid Friction Coefficient, Society of Petroleum Engineers, SPE Annual Technical Conference and Exhibition, 8–11 October, San Antonio, TX, 1989, https://doi.org/10.2118/19537-MS.
[89] G.D. Alshubbar, T.N. Coryell, A. Atashnezhad, S. Akhtarmanesh, G. Hareland, The Effect of Barite Nanoparticles on the Friction Coefficient and Rheology of Water Based Mud, American Rock Mechanics Association, 51st U.S. Rock Mechanics/Geomechanics Symposium, 25–28 June, San Francisco, CA, USA, 2017 https://www.onepetro.org/conference-paper/ARMA-2017-0147.
[90] M.T. Al-saba, A.A. Fadhli, A. Marafi, A. Hussain, F. Bander, M.F.A. Dushaishi, Application of Nanoparticles in Improving Rheological Properties of Water Based Drilling Fluids, Society of Petroleum Engineers, SPE Kingdom of Saudi Arabia Annual Technical Symposium and Exhibition, 23–26 April, Dammam, Saudi Arabia, 2018, https://doi.org/10.2118/192239-MS.
[91] G. Altun, A.E. Osgouei, M.H. Ozyurtkan, An Alternate Mud Proposal to Minimise Borehole Instability, International Petroleum Technology Conference, International Petroleum Technology Conference, 10–12 December, Kuala Lumpur, Malaysia, 2014, https://doi.org/10.2523/IPTC-17871-MS.
[92] B.I. Routh, B.C. Craft, Effect of Temperature on the Gel Strength of Some Gulf Coast Drilling Muds, Society of Petroleum Engineers, Petroleum Technology, 1938, pp. 1–7, https://doi.org/10.2118/938082-G.
[93] E.C. Bingham, An Investigation of the Laws of Plastic Flow vol. 13, US Bureau of Standards Bulletin, 1916, pp. 309–353, https://doi.org/10.6028/bulletin.304.
[94] W.H. Herschel, R. Bulkley, Konsistenzmessungen von Gummi-Benzollösungen, Kolloid Zeitschrift 39 (4) (1926) 291–300, https://doi.org/10.1007/BF01432034.
[95] W. Ostwald, de Waele-Ostwald equation, Kolloid Zeitschrift 47 (2) (1929) 176–187.
[96] S. Forthun, M. Belayneh, The effect of MoS2 nanoparticle on the properties & performance of XG polymer/salt treated bentonite drilling fluid, Int. J. NanoSci. Nanotechnol. 8 (1) (2017) 49–58.
[97] Scomi, Drilling Fluids, (2019) (online; accessed January 2019), http://scomigroup.com.my/GUI/pdf/drilling_fluid.pdf.
[98] M. Li, S. Deng, F. Meng, J. Hao, X. Guo, Effect of nanosilica on the mechanical properties of oil well cement at low temperature, Mag. Concr. Res. 69 (10) (2017) 493–501, https://doi.org/10.1680/jmacr.16.00394.
[99] Mustafa Versan Kok, Berk Bal, Effects of silica nanoparticles on the performance of water-based drilling fluids, Journal of Petroleum Science and Engineering 180 (2019) 605–614.

Allan Katende is born and raised in Uganda, educated in a British and Norwegian school system. At the time of publication, he holds an Msc. Petroleum Engineering with great honour from the Norwegian University of Science and Technology in 2015 and a Bsc. Mechanical Engineering (**Magna Cumlaude**) where he graduated as a valedictorian from Makerere University, College of Engineering, Design, Art and Technology in 2013. He has several industry experience on Oil and Gas Exploration, Production and Recovery from the Norwegian Continental Shelf, Shale Oil & Gas production in Texas, USA and in Uganda. He is actively involved in both teaching and research and his research and teaching interests include but not limited to; Drilling Engineering with emphasis on Drilling Fluids, Hole Cleaning, Well Control, Well Construction and Well Integrity; Fluid Flow and Transport in Porous Media; Experimental and Numerical Simulation of Enhanced Oil Recovery methods; Nanotechnology and its applications in Engineering; Thermodynamics; Materials Science; Fractured Reservoirs; Shale Well Modeling and Decline Curve Analysis; Data driven modeling; Petrophysics; Physiochemical and Environmental Engineering; Fluid Mechanics; Multiphase Flow, Production Engineering, Engineering Mechanics & Mechanics of Materials. He has also worked at the Department of Geoscience and Petroleum Engineering at the Norwegian University of Science and Technology as a graduate teaching assistant for Fractured Reservoirs.

Natalie V. Boyou holds a PhD in Petroleum Engineering from Universiti Teknologi Malaysia. She also holds a bachelors degree in Physics and a masters degree in Petroleum Engineering. She has experience in reliability and maintenance of offshore and onshore platforms. She carried out her research attachment in University of Aberdeen whilst doing her doctorate. Her research interests include, but not limited to application of nanotechnology in drilling fluid, degradation of drilling fluid, cuttings transportation, and non-Newtonian fluid rheology.

Issham Ismail is an Associate Professor at Department of Petroleum Engineering, Universiti Teknologi Malaysia. He is also a Chartered Engineer of the UK Council and Institute of Marine, Science and Technology. His research interests are in well completion, formation evaluation, drilling fluid, hole cleaning, petroleum production, applications of nanotechnology in petroleum engineering, and flow assurance. He is actively involved in both teaching and research, and has published many novelty articles in international journals. His great achievement is the publication of single authored three well completion and slickline operations books by UTM Press.

Derek Z. Chung holds petroleum engineering degrees from the University of Teknologi Malaysia. He is working as a Completions Field Engineer with Schlumberger. His research interests include well completion and wellbore cleaning.

Farad Sagala is currently pursuing a PhD in Petroleum Engineering at the University of Calgary focussing on applications of nanoparticles for enhancing oil recovery. He holds an Msc in Petroleum Engineering (Summa Cumlaude) from the University of Technology Malaysia in 2015 and a Bsc. in Bio-systems and Mechanical Engineering from Makerere University in 2013. He has knowledge on using various Experimental and simulations techniques with use of various softwares across the petroleum engineering value chain. His Research interests involve the applications of nanoparticles for enhancing recovery in the oil and gas industry.

Norhafizuddin Hussein holds an MSc in Petrolem Engineering by Universiti Teknologi Malaysia. He is currently pursuing a PhD in Petroleum Engineering at the Universiti Teknologi Malaysia focussing on flow assurance.

Muhamad S. Ismail holds an MSc in Petrolem Engineering by Universiti Teknologi Malaysia. He is currently working as a Cementing Technical Engineer at Setegap Ventures Petroleum Sdn. Bhd. His research interests include cementing, drilling fluids and wellbore cleaning.